Ocean Alkalinity Enhancement - Avoiding runaway $CaCO_3$ precipitation during quick and hydrated lime dissolution

Charly A. Moras[1,*], Lennart T. Bach[2], Tyler Cyronak[3], Renaud Joannes-Boyau[1], Kai G. Schulz[1]

[1]Faculty of Science and Engineering, Southern Cross University, Lismore, NSW, Australia
[2]Institute for Marine and Antarctic Studies, Ecology & Biodiversity, University of Tasmania, Hobart, TAS, Australia
[3]Department of Marine and Environmental Sciences, Nova Southeastern University, Fort Lauderdale, FL, USA

* *Correspondence to:* Charly A. Moras (c.moras.10@student.scu.edu.au)

Abstract. Ocean Alkalinity Enhancement (OAE) has been proposed as a method to remove carbon dioxide (CO_2) from the atmosphere and to counteract ocean acidification. It involves the dissolution of alkaline minerals. However, a critical knowledge gap exists regarding their dissolution in natural seawater. Particularly, how much alkaline mineral can be dissolved before secondary precipitation of calcium carbonate ($CaCO_3$) occurs is yet to be established. Secondary precipitation should be avoided as it reduces the atmospheric CO_2 uptake potential of OAE. Using two proposed OAE minerals as example, i.e., quick lime (CaO) and hydrated lime ($Ca(OH)_2$), we show that both feedstocks (<63 µm of diameter) dissolved in seawater within a few hours. However, while no $CaCO_3$ precipitation was found to occur at a saturation state (Ω_{Ar}) of about 5, $CaCO_3$ precipitated in the form of aragonite beyond a threshold of 7. This limit is much lower than what would be expected for typical pseudo-homogeneous precipitation in the presence of colloids and organic matter. Secondary precipitation at unexpectedly low Ω_{Ar} was the result of so-called heterogeneous precipitation onto mineral phases, most likely onto CaO and $Ca(OH)_2$ prior to full dissolution. Most importantly, this led to runaway $CaCO_3$ precipitation, i.e., significantly more alkalinity (TA) was removed than initially added, until Ω_{Ar} reached levels below 2. Such runaway precipitation would reduce the CO_2 uptake efficiency from about 0.8 moles of CO_2 per mole of TA down to only 0.1 mole of CO_2 per mole of TA. Runaway precipitation appears to be avoidable by dilution below the critical Ω_{Ar} threshold of 5, ideally within hours of the addition to minimise initial $CaCO_3$ precipitation. Finally, OAE simulations suggest that for the same Ω_{Ar} threshold, the amount of TA that can be added to seawater would be more than three times higher at 5 °C than at 30 °C. Also, equilibration to atmospheric CO_2 levels, i.e., to a pCO_2 of ~416 µatm, during mineral dissolution would further increase it by a factor of ~6 and ~3 respectively.

1 Introduction

30   Climate change is currently considered one of the greatest threats to humankind (Hoegh-Guldberg et al., 2019; IPCC, 2021; The Royal Society and Royal Academy of Engineering., 2018). Global mean temperature has increased by 1.0 °C since pre-industrial times, and could reach +1.2-1.9 °C in the next 20 years, and +2.1-5.7 °C by the end of this century (IPCC, 2021). Furthermore, up to 30% of anthropogenic CO_2 emissions have been taken up by the ocean through air-sea gas exchange, leading to a decrease in the average open ocean pH by 0.1 units in a process termed ocean acidification – OA (Bates et al.,

35   2012; Canadell et al., 2007; Carter et al., 2019; Cyronak et al., 2014; Doney et al., 2009; Hoegh-Guldberg et al., 2007).

      The CO_2 reduction pledges by the signatory states of the 2015 Paris Agreement aim to minimise the negative impacts of global warming and OA on ecosystems and human societies by limiting warming to less than +2.0 °C, ideally below +1.5 °C, by the end of this century (Goodwin et al., 2018). However, current and pledged reductions will likely not be enough and additional mitigation strategies are being discussed, such as ocean alkalinity enhancement – OAE (Boyd et al., 2019; Gattuso

40   et al., 2015; Lenton and Vaughan, 2009; The Royal Society and Royal Academy of Engineering., 2018). Among carbon dioxide removal approaches, OAE has a high carbon dioxide removal potential, with models suggesting that between 165 and 790 Gigatonnes (1 Gt = 1e15 g) of atmospheric CO_2 could be removed by 2100 on a global scale (Burt et al., 2021; Feng et al., 2017; Keller et al., 2014; Köhler et al., 2013; Lenton et al., 2018). However, there is no empirical data on OAE efficacies, in particular regarding safe thresholds for mineral dissolution (National Academies of Sciences and Medicine, 2021).

45   OAE typically relies on the dissolution of alkaline minerals in seawater, releasing alkalinity similarly to natural rock weathering (Kheshgi, 1995). Suitable candidates are magnesium-rich minerals such as brucite, periclase or forsterite, and calcium-rich minerals such as quick and hydrated lime (Renforth and Henderson, 2017). Quick and hydrated lime are of particular interest, due to their high solubility in seawater as well as their relatively rapid dissolution. Quick lime, also known as calcium oxide (CaO), is obtained by the calcination of limestone, mainly composed of calcium carbonate ($CaCO_3$) and

50   present in large quantities in the Earth's crust. Once heated to temperatures of ~1200 °C, each molecule of $CaCO_3$ breaks down into one molecule of CaO and one molecule of CO_2 (Ilyina et al., 2013; Kheshgi, 1995). Hence, for maximum OAE potential, carbon capture during calcination and subsequent storage would be advisable (Bach et al., 2019; Ilyina et al., 2013; Kheshgi, 1995; Renforth et al., 2013; Renforth and Kruger, 2013). CaO can then be hydrated into calcium hydroxide ($Ca(OH)_2$), also known as hydrated lime. The addition of either CaO or $Ca(OH)_2$ to seawater leads to the dissociation of $Ca(OH)_2$ into one

55   calcium Ca^{2+} and two hydroxyl ions OH^- (Feng et al., 2017; Harvey, 2008). The chemical reaction of CO_2 and $Ca(OH)_2$ dissolution can be written as follows, which includes the subsequent uptake of atmospheric CO_2, and ignores the non-linearities of the seawater carbonate system (i.e., changes in total alkalinity, TA, and dissolved inorganic carbon, DIC, are not 1:1):

$$(CaO + H_2O \rightleftharpoons Ca(OH)_2) + 2CO_2 \rightarrow Ca^{2+} + 2HCO_3^- \qquad\qquad 1$$
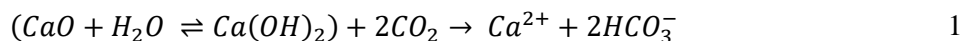
60

The dissolution of CaO and Ca(OH)$_2$ and the subsequent addition of TA increases seawater pH, while changing the carbonate chemistry speciation. DIC can be approximated by being the sum of HCO$_3^-$ and CO$_3^{2-}$ (ignoring the relatively small contribution by CO$_2$). Similarly, TA can be approximated as the sum of HCO$_3^-$ and 2 CO$_3^{2-}$ (ignoring the smaller contributions by boric and silicic acid, and other minor components). Combining both DIC and TA equations reveal that CO$_3^{2-}$ concentrations can be expressed as [CO$_3^{2-}$] = TA-DIC. Hence, increasing TA at constant DIC, e.g., by dissolving CaO or Ca(OH)$_2$, increases [CO$_3^{2-}$], shifting carbonate chemistry speciation towards higher pH (Figure A 1) (Dickson et al., 2007; Wolf-Gladrow et al., 2007; Zeebe and Wolf-Gladrow, 2001). The shift in DIC speciation leads to a decrease in [CO$_2$], reducing the partial pressure of CO$_2$ (pCO$_2$) in seawater and increasing its atmospheric CO$_2$ uptake potential.

Depending on the amount of TA added and the initial seawater pCO$_2$, the TA-enriched seawater would either take up CO$_2$ from the atmosphere or reduce outgassing of CO$_2$ in the case where seawater pCO$_2$ is still above atmospheric levels. Factoring in carbonate system non-linearities, about 1.6 moles of atmospheric CO$_2$ could be taken up per mole of CaO or Ca(OH)$_2$ (Köhler et al., 2010). Furthermore, dissolving CaO and Ca(OH)$_2$ can also counteract ocean acidification in two ways, raising the pH and the calcium carbonate saturation state of seawater (Ω_{CaCO3}), with Ω_{CaCO3} increasing both because of increased [Ca^{2+}] and [CO$_3^{2-}$]. This makes OAE a dual solution for removing atmospheric CO$_2$ and mitigating OA (Boyd et al., 2019; Feng et al., 2017; Harvey, 2008). However, major knowledge gaps exist regarding OAE, considering most research to date has been based on conceptual and numerical modelling (Feng et al., 2016; González and Ilyina, 2016; Mongin et al., 2021; Renforth and Henderson, 2017).

One such knowledge gap is the critical Ω_{CaCO3} threshold that seawater can be raised to beyond which CaCO$_3$ would precipitate inorganically. Such secondary precipitation constitutes the opposite of alkaline mineral dissolution and would decrease pH and Ω_{CaCO3}, simultaneously increasing seawater [CO$_2$]. This would decrease the ocean uptake's capacity for atmospheric CO$_2$, having the opposite effect as what is initially intended. Similarly, if all added alkalinity is being precipitated, only 1 mole of atmospheric CO$_2$ per mole of Ca^{2+} would be removed, instead of about 1.6 without. If even more CaCO$_3$ precipitates, the efficiency would be further reduced. CaCO$_3$ does not precipitate spontaneously in typical seawater due to various factors such as the absence of mineral phase precipitation nuclei and the presence of precipitation inhibitors such as dissolved organic compounds, magnesium or phosphate (Chave and Suess, 1970; De Choudens-Sanchez and Gonzalez, 2009; Pytkowicz, 1965; Rushdi et al., 1992; Simkiss, 1964). The latter two directly influence CaCO$_3$ nuclei formation rates. There are three types of precipitation, i.e., 1) homogeneous (in the absence of any precipitation nuclei), 2) heterogeneous (in the presence of mineral phases), and 3) pseudo-homogeneous (in the presence of colloids and organic materials) (Marion et al., 2009; Morse and He, 1993). For the latter, the critical precipitation threshold for calcite (at a salinity of 35 and at a temperature of 21 °C) is at a saturation state (Ω_{Ca}) of ~18.8 (Marion et al., 2009). Assuming a typical open-ocean TA and DIC concentrations, i.e., ~2350 µmol kg^{-1} and ~2100 µmol kg^{-1} respectively (Dickson et al., 2007), this threshold would be reached by an increase in TA of ~810 µmol kg^{-1}, corresponding to a critical threshold for Ω_{CaCO3} with respect to aragonite, i.e., Ω_{Ar}, of ~12.3. Concerning the two other types of precipitation, i.e., homogeneous and heterogeneous, these are poorly constrained

(Marion et al., 2009). Importantly, at the current seawater dissolved magnesium concentration, the $CaCO_3$ morphotype that is favoured during inorganic precipitation is aragonite rather than calcite (Morse et al., 1997; Pan et al., 2021).

To gain a better understanding, we conducted several dissolution experiments with CaO and $Ca(OH)_2$ to determine 1) how much alkaline material can be dissolved without inducing $CaCO_3$ precipitation, 2) what causes secondary $CaCO_3$ precipitation, and 3) how secondary precipitation can be avoided if observed.

2 Material & Methods

2.1 Experimental setup

Two different calcium minerals were used, CaO powder from Ajax Finechem (CAS no 1305-78-8) and an industrial $Ca(OH)_2$ powder (Hydrated Lime 20kg, Dingo). The elemental composition of these powders was analysed on an Agilent 7700 Inductively Coupled Plasma Mass Spectrometer, coupled to a laser ablation unit NWR213 from Electro Scientific Industries, Inc. The samples were embedded in resin and calibrated against standard reference materials #610 and #612 from the National Institute of Standards and Technology.

The dissolution experiments were conducted in natural seawater. The seawater was collected between September 2020 and June 2021, about 200 to 300 m from the shore, avoiding suspended sand or silt, at Broken Head, New South Wales, Australia (28°42'12" S, 153°37'03" E). Seawater was stored up to 14 days at 4 °C in the dark to slow bacterial metabolic activity and allow for all particles in suspension to sink to the bottom before being sterile-filtered using a peristaltic pump, connected to a 0.2 µm Whatman Polycap 75 AS filter. For salinity measurements, about 200 mL of seawater were placed in a gas-tight polycarbonate container and allowed to equilibrate to room temperature overnight. The sample's conductivity was then measured using a measuring cell (Metrohm 6.017.080), connected to a 914 pH/Conductometer. The conductivity was recorded in millisiemens per cm (mS/cm), and the temperature in °C. Salinity was calculated according to Lewis and Perkin (1981) on the 1978 practical salinity scale. The salinity in each experiment is reported in Table A 1.

2.2 OAE experiments

For each experiment, seawater was accurately weighed (in grams to 2 decimal places) into high-quality borosilicate 3.3 2L Schott Duran beakers, and the temperature was controlled via a Tank Chiller Line TK 1000 set to 21 °C, feeding a re-circulation water jacket (Figure A 2). A magnetic stir bar was placed in the beaker, and the natural seawater was constantly stirred at ~200 rpm. To minimise gas exchange, a floating lid with various sampling ports was placed on top. Finally, after one hour of equilibration, calculated amounts of weighed-in alkaline compounds were added. Upon addition, samples for DIC and TA were taken at increasing time intervals to fully capture the dissolution kinetics and check for potential secondary precipitation. Furthermore, the pH was monitored at a frequency of 1 Hertz for the first hour before alkalinity addition, and over 4 hours after addition to get an estimate for when alkalinity was fully released. Once the pH plateaued (corresponding to maximum TA release), the content of the beaker was carefully transferred to a clean Schott bottle to ensure that evaporation would not

play a role in changing DIC and TA. Bottles were kept in the dark for the duration of each experiment, i.e., up to 48 days, with the same constant stirring of ~200 rpm at 21 °C. Each bottle was exposed to UV light for at least 30 minutes after each sampling to avoid bacterial growth.

2.2.1 CaO and Ca(OH)$_2$ dissolution

Following the previously described beaker setup, TA was added by sieving CaO and Ca(OH)$_2$ through a 63 µm mesh, avoiding the formation of larger CaO or Ca(OH)$_2$ aggregates. The mesh was placed in a clean upside-down 50 mL Falcon tube cap, to minimise the loss of material smaller than 63 µm, and the overall weight was recorded in mg. Then, the mesh was placed above the Schott bottle, and mineral was added by gently tapping the side of the sieve. Finally, the sieve was placed in the same upside-down Falcon tube cap and weighed once again, thereby making sure that the desired amount had been added to the beaker. The weighing steps were carefully performed to avoid material loss between the bottle and the balance, and was achieved in less than 5 min. Two alkalinity additions, +250 and +500 µmol kg^{-1} with each calcium mineral powder were performed (Table 1).

2.2.2 Na$_2$CO$_3$ alkalinity and particles additions, and filtration

Three further experiments assessed the role of mineral phases during secondary CaCO$_3$ precipitation observed in the previous experiments. The first experiment made use of a 1M solution of sodium carbonate (Na$_2$CO$_3$, CAS number 497-19-8) which was freshly prepared before the experiment. Ultrapure Na$_2$CO$_3$ was accurately weighed, i.e., in mg (with 2 decimal places), into a clean 100 mL Schott bottle and made up to 100 g with MilliQ (18.2 MΩ). The solution was then sonicated for 15 minutes, and gentle mixing every five minutes. The amount of Na$_2$CO$_3$ to be added to seawater was calculated so that a similar maximum Ω_{Ar} would be reached, i.e., ~7.7, as in the previous experiments with the highest addition of CaO and Ca(OH)$_2$. This required about twice the alkalinity increase as before (Table 1), because Na$_2$CO$_3$ additions concomitantly increase DIC when dissociating in two sodium and one CO$_3^{2-}$ ion, making the Ω_{CaCO3} increase smaller. All carbonate chemistry calculations were done in CO$_2$SYS (see below).

In another similar experiment to the Na$_2$CO$_3$ addition, quartz powder was added after two days. Quartz powder was chosen as it does not dissolve on the timescales relevant for this study (Montserrat et al., 2017). The addition of quartz powder was similar to the sieved CaO and Ca(OH)$_2$ additions, i.e., through a 63 µm mesh. The mass of quartz particles added, recorded in mg, was determined to provide the same mineral surface area as for the Ca(OH)$_2$ experiments with a TA increase of 500 µmol kg^{-1}. It was calculated using densities and masses for Ca(OH)$_2$ and quartz, and assuming spherical particles with a diameter of 63 µm.

Finally, a third experiment was carried out in which all particles were removed by filtration, using Ca(OH)$_2$ as the alkaline compound and following the same setup as described above (section 2.2.1). Here we first added Ca(OH)$_2$ to increase TA by ~500 µmol kg^{-1} (Table 1). After 4h of reaction, the entire content of the 2L Schott beaker was filtered through a nylon

Captiva Econofilter (25mm) with a pore size of 0.45 µm into a clean 1L Schott bottle using a peristaltic pump. The bottle was filled from bottom to top, with overflow to minimise gas exchange.

2.2.3 Dilution experiments

In a last set of experiments, alkalinity enriched seawater was diluted with natural seawater, to test if secondary precipitation can be avoided or stopped. $Ca(OH)_2$ powder was added to reach final alkalinity enrichments of 500 and 2000 µmol kg^{-1} and dilutions were carried out at several points in time.

For the experiment with a targeted TA increase of 500 µmol kg^{-1}, a larger quantity of TA enriched seawater was required to perform all dilutions and sampling in comparison to the previous experiments. Therefore, two 5L Schott bottles were filled with 5kg of natural seawater and placed on a magnetic stirring platform. Calculated weighed-in masses of $Ca(OH)_2$ were added to the first bottle as described in section 2.2.1 using the 63 µm sieve, while the natural seawater in the second bottle was kept for subsequent dilutions. Both bottles were kept on the same bench under the same conditions, both stirring at a rate of ~200 rpm, for the duration of the experiment.

Following the $Ca(OH)_2$ addition, 1:1 dilutions (500 g TA enriched seawater:500 g natural seawater) were performed in clean 1L Schott bottles that were then kept in the dark and placed on a magnetic platform at a stirring rate of ~200 rpm. After each sampling, the bottles were exposed to UV light for at least 30 minutes. The second dilution experiment was set up like the first one, the only difference being that the targeted TA increase was 2000 µmol kg^{-1}. The dilution ratio was 1:7 to reduce the targeted TA increase again to 250 µmol kg^{-1}. All dilutions were performed 10 minutes, 1 hour, 1 day and 1 week after $Ca(OH)_2$ addition, leading to 2 TA-enriched and 8 diluted treatments.

2.3 Carbonate chemistry measurements

Samples for TA and DIC measurements were filtered through a nylon Captiva Econofilter (0.45 µm) using a peristaltic pump into 100 mL Borosilicate 3.3 Schott DURAN glass stopper bottles. The bottles were gently filled from the bottom to top, using a 14-gauge needle as described in Schulz et al. (2017), with at least half of their volume allowed to overflow, corresponding to ~150 mL of seawater sampled per time-point (Dickson et al., 2007). After filling, 50µL of saturated mercuric chloride solution was added to each sample before being stored without headspace in the dark at 4 °C.

TA was analysed in duplicates via potentiometric titrations on an 848 Titrino Plus coupled to an 869 Compact Sample Changer from Metrohm using 0.05M HCl, with the ionic strength adjusted to 0.72 mol kg^{-1} with NaCl, corresponding to a salinity of 35. Titrations and calculations followed the open-cell titration protocols by Dickson et al. (2007). DIC was measured in triplicates using an Automated Infra-Red Inorganic Carbon Analyzer (AIRICA) coupled to a LICOR Li7000 Infra-Red detector as described in Gafar and Schulz (2018). Measured values of TA and DIC were corrected using an internal Standard prepared as per Dickson et al. (2007) which had been calibrated against Certified Reference Materials Batch #175 and #190 (Dickson, 2010).

2.4 Particulate Inorganic Carbon and Scanning Electron Microscopy (SEM)

In cases where TA and DIC decreases were detected, indicative of $CaCO_3$ precipitation, several samples were taken at the end of the experiments for total particulate carbon (TPC), particulate organic carbon (POC) and scanning electron microscopy (SEM) analyses. TPC and POC samples were collected in duplicates on pre-combusted (450 °C) GF/F filters and stored frozen until analysis. Before analysis, POC filters were fumed with HCl for 2 hours before drying over night at 60 °C while TPC filters were dried untreated (Gafar and Schulz, 2018). The filters were wrapped in tin capsules and pressed into small balls of about 5mm diameter. Both TPC and POC were quantified on an Elemental Analyser Flash EA, Thermo Fisher, coupled to an Isotope Ratio Mass Spectrometer, Delta V Plus. Particulate inorganic carbon (PIC), or $CaCO_3$, was calculated from the difference between TPC and POC. The results are reported in $\mu mol\ kg^{-1}$ with an uncertainty estimate for each calculated by an error propagation from the square root of the sum of the squared standard deviations for TPC and POC.

For SEM analysis, 10 to 15 mL of the sample water was collected on polycarbonate Whatman Cyclopore filters with a 0.2 µm pore size, and rinsed with 50 mL of MilliQ. The filters were dried at 60 °C overnight and kept in a desiccator until analysis on a tabletop Scanning Electron Microscope TM4000 Plus from Hitachi, coupled to an Energy Dispersive X-Ray (EDX) Analyser, allowing to identify the morphotype and elemental composition of precipitates. Finally, CaO and $Ca(OH)_2$ powders were analysed for their carbon content. This analysis aimed to identify the presence and estimate the amount of particulate carbon, most likely $CaCO_3$, in the respective mineral powders.

2.5 Carbonate chemistry calculations

Measured DIC, TA, temperature and salinity were used to calculate the remaining carbonate chemistry parameters with the CO_2SYS script for MATLAB® (MathWorks). The borate to salinity relationship from Uppstrom (1974), dissociation constants for carbonic acid by Lueker et al. (2000), and for boric acid by Uppstrom (1974) were used. With two measured carbonate chemistry parameters, i.e., DIC and TA, the others can be calculated straight away. An exception in our experiments was that the dissolution of CaO and $Ca(OH)_2$ changes the calcium concentration and hence the salinity-based Ω_{CaCO3} calculated by CO_2SYS is underestimated. Ω_{CaCO3} is defined by the solubility product of $CaCO_3$ as:

$$\Omega_{CaCO3} = \frac{[Ca^{2+}] \times [CO_3^{2-}]}{K_{sp}} \qquad 2$$

where $[Ca^{2+}]$ and $[CO_3^{2-}]$ denote seawater concentration of Ca^{2+} and CO_3^{2-}, and K_{sp} the solubility product for calcite or aragonite. To calculate saturation states, the correct calcium concentration $[Ca^{2+}]_{Corr}$ was estimated from measured salinity (Riley and Tongudai, 1967) and half the alkalinity concentration increase that was generated during CaO or $Ca(OH)_2$ dissolution or lost due to $CaCO_3$ precipitation, ΔTA:

$$[Ca^{2+}]_{Corr} = \frac{0.01028}{35} \times \text{Salinity} + \frac{\Delta TA}{2} \qquad\qquad 3$$

where 0.01028 denotes molar Ca^{2+} concentrations at a salinity of 35. K_{sp} was calculated from in-situ temperature and salinity according to Mucci (1983). The corrected Ω_{Ca} and Ω_{Ar} were then calculated according to Equation 2. Please note that we have

220   opted to report Ω_{Ar} rather than Ω_{Ca} since aragonite is more likely to be precipitated in natural modern seawater (Berner, 1975; Morse et al., 1997; Riebesell et al., 2011; Zeebe and Wolf-Gladrow, 2001).

2.6 OAE simulations

CO2SYS and the results from the various dissolution experiments were used to simulate three OAE scenarios (Table 3). Three alkalinity additions were simulated, +250, +500 and +1000 µmol kg^{-1}. The starting parameters were TA = 2350 µmol

225   kg^{-1}, DIC = 2100 µmol kg^{-1}, salinity = 35, temperature = 19 °C, using the same acid-base equilibrium constants as described in section 2.5. In the first scenario, for all three additions, no $CaCO_3$ precipitation was assumed, and the amount of CO_2 taken up after atmospheric re-equilibration was calculated. For the +500 and +1000 µmol kg^{-1} TA increases, two additional simulations were performed: first we assumed that as much $CaCO_3$ precipitated as TA was added, and second, that $CaCO_3$ precipitated down to an Ω_{Ar} of ~2 as observed in our experiments. Again, after calculating full carbonate chemistry speciation

230   in these various scenarios, the amount of CO_2 taken up after atmospheric re-equilibration was determined.

3 Results

3.1 Chemical composition of CaO and Ca(OH)$_2$

The chemical composition of the CaO and Ca(OH)$_2$ powders were analysed for their major ions. As to be expected, both consisted mainly of calcium, with minor contributions of magnesium and silicon (see Table A 2, for a more comprehensive

235   list). Furthermore, CaO and Ca(OH)$_2$ contained about 9.4 ±0.1 mg g^{-1} and 18.0 ±0.2 mg g^{-1} of particulate carbon respectively, i.e., ~0.9% and ~1.8% by weight.

3.2 CaO dissolution in filtered natural seawater

In the first CaO experiment with a targeted 250 µmol kg^{-1} TA addition, TA increased by ~200 µmol kg^{-1} within the first 4 hours (Figure 1a). Following this increase, TA was stable over time. In contrast, DIC increased slowly, about 1 µmol

240   kg^{-1} per day, reaching about +50 µmol kg^{-1} on day 47 of the experiment (Figure 1b). Ω_{Ar} reflected the trend observed for ΔTA, increasing from ~2.9 to ~5.1 within the first 4 hours before slowly decreasing to 5.0 on day 47 (Figure 1c).

In the second CaO experiment with a targeted 500 µmol kg^{-1} TA addition, TA increased by ~410 µmol kg^{-1} within the first 4 hours before slowly decreasing on day 3 (Figure 1a), followed by a more rapid decrease over the following week, before eventually reaching a steady state on day 20 at a final ΔTA of about -540 µmol kg^{-1}. This corresponds to a total loss of

TA of ~950 µmol kg^{-1}, between the maximum measured TA and the final TA recorded. Similarly, a relatively small decrease in DIC of ~10 µmol kg^{-1} was observed over the first two days before a much more significant reduction in the following week before levelling off at a ΔDIC of about -465 µmol kg^{-1} (Figure 1b). Ω_{Ar} increased rapidly during the first 4 hours of the experiment from 2.8 up to 7.6 (Figure 1c). Following this quick increase, Ω_{Ar} decreased by 0.3 units by day 3. Afterwards, Ω_{Ar} dropped quickly to 2.4 on day 13, and reached ~1.8 on day 47, corresponding to a reduction by 1.0 compared to the starting seawater value.

3.3 Ca(OH)$_2$ dissolution in filtered natural seawater

In the first Ca(OH)$_2$ experiment with a targeted TA addition of 250 µmol kg^{-1}, TA increased by ~220 µmol kg^{-1} after 4h of reaction, before stabilising at a ΔTA of ~210 µmol kg^{-1} for the rest of the experiment (Figure 2a). The DIC concentration increased relatively quickly over the first 6 days after the TA addition before slowing down, reaching about +70 µmol kg^{-1} by the end of the experiment (Figure 2b). Finally, Ω_{Ar} reached ~4.1 after 4 hours, slightly decreasing over time, down to 3.3 on day 28 (Figure 2c).

In the second Ca(OH)$_2$ experiment with a targeted TA addition of 500 µmol kg^{-1}, TA increased by ~440 µmol kg^{-1} within the first 4h (Figure 2a). This was followed by a relatively steady decrease by ~18 µmol kg^{-1} per day over the next 2 weeks, after which the decrease accelerated to ~28 µmol kg^{-1} per day until day 35, before levelling off at a ΔTA of about -420 µmol kg^{-1} towards the end of the experiment. Overall, about 860 µmol kg^{-1} of TA was lost compared to the highest TA recorded. The DIC concentration decreased as well, dropping in a similar fashion as TA and reaching a ΔDIC of about -395 µmol kg^{-1} compared to the initial DIC concentration (Figure 2b). Ω_{Ar} increased from 2.5 to 7.4 in the first 4 hours before decreasing, similarly to TA and DIC, reaching ~2.0 on day 42 (Figure 2c).

3.4 Na$_2$CO$_3$, particle addition and filtration

Three experiments assessed the influence of particles on CaCO$_3$ precipitation. In the first one, ~1050 µmol kg^{-1} of TA was added using a 1M Na$_2$CO$_3$ solution, designed to result in a similar maximum Ω_{Ar} as in the previous experiments when TA decreased (Table 1). Upon addition, TA increased by ~1060 µmol kg$^-$ and DIC by ~530 µmol kg^{-1} within minutes. For the remainder of the experiment, ΔTA was fairly constant between 1060 and 1040 µmol kg^{-1} (Figure 3a). In contrast, DIC slightly increased over 42 days from a ΔDIC of ~530 µmol kg^{-1} on day 1 to ~560 µmol kg^{-1} on day 42 (Figure 3b). Ω_{Ar} increased from ~2.3 to ~8.5 within minutes and slightly decreased to ~8.1 after 42 days of experiment (Figure 3c).

In the second experiment, the addition of 1M Na$_2$CO$_3$ solution (Table 1) increased TA by 1070 µmol kg^{-1}, while DIC increased by ~540 µmol kg^{-1} within minutes and remained stable (Figure 3a, 3b). After 2 days, quartz particles were added. While one day later ΔTA and ΔDIC remained unchanged, between day 5 and 12 ΔTA decreased to ~220 µmol kg^{-1} and ΔDIC dropped to ~120 µmol kg^{-1} (Figure 3a, 3b). Over the next month, ΔTA and ΔDIC continued to decrease, although at a slowing rate, reaching about -200 and -110 µmol kg^{-1}, respectively, at the end of the study. Ω_{Ar} followed a similar trend, with an

increase from ~2.8 up to ~9.2 within the first 1.5 hours, and a pronounced decline to ~3.9 between day 5 and day 12, before stabilizing around ~2.0 at the end of the experiment.

In the last experiment, $Ca(OH)_2$ was added aiming for a TA increase of 500 µmol kg^{-1} (Table 1), a level at which a significant TA decrease had been observed previously (Figure 2a). In contrast however, upon filtration of the entire experimental bottle content after reaching ~470 µmol kg^{-1} at the 4-hour mark, ΔTA remained relatively constant between 465 and 470 µmol kg^{-1} over the following 48 days of experiment (Figure 3a). At the same time, ΔDIC increased from ~5 to 55 µmol kg^{-1} after filtration (Figure 3b). Ω_{Ar} increased from ~2.8 to ~8.2 within the first 1.5 hours, and then slightly decreased to ~7.5 over the 48 days of experiment (Figure 3c).

3.5 Dilution experiments

3.5.1 500 µmol kg^{-1} addition

In these experiments with a targeted TA addition of 500 µmol kg^{-1} by $Ca(OH)_2$, ΔTA increased to ~450 µmol kg^{-1} after 2 hours (Figure 4). These changes in TA were followed by a decline to ~320 µmol kg^{-1} after 14 days, although the latter being a slightly slower decrease than previously (Figure 2Figure 4a). After a first increase in ΔDIC by ~10 µmol kg^{-1} on day 1, DIC steadily decreased to about -20 µmol kg^{-1} after two weeks (Figure 4b). Finally, Ω_{Ar} increased from ~2.7 to ~7.8 after 2 hours, before steadily decreasing to ~6.4 on day 14 (Figure 4c).

In the diluted treatments, ΔTA remained relatively stable over time, until the end of the experiments on day 29, regardless of dilution time (Figure 4a). Upon dilution, ΔTA was reduced, being very similar for the 10 minutes, 1 hour and 1 day dilutions. Overall, in the 1 week dilution, ΔTA was slightly lower, i.e., ~205 µmol kg^{-1} instead of ~230 µmol kg^{-1} on average. In all dilutions, ΔDIC increased over time, ranging between ~20 µmol kg^{-1} and ~60 µmol kg^{-1}, independent of dilution timing. Finally, Ω_{Ar} showed similar trends like ΔTA, reaching between ~4.8 and ~5.2, and slightly decreasing over time until end of the experiment.

3.5.2 2000 µmol kg^{-1} addition

This set of experiments aimed for a TA increase of 2000 µmol kg^{-1} by $Ca(OH)_2$ addition. However, the TA only increased to ~⅓ of the theoretical value, i.e., ~725 µmol kg^{-1} within the first two hours (Figure 4d). Following this increase, TA rapidly decreased during the first day, reaching a ΔTA of about -1260 µmol kg^{-1}, and -1440 µmol kg^{-1} in the following week (Figure 4d). Over the second week of the experiment, TA appeared to stabilise before slightly increasing until day 21. In contrast, ΔDIC decreased by ~580 µmol kg^{-1} already within the first two hours, before rapidly dropping to about -1590 µmol kg^{-1} on day 1, and -1660 µmol kg^{-1} after 7 days (Figure 4e). Over the remaining 41 days, ΔDIC then increased by ~210 µmol kg^{-1}, although remaining about 1450 µmol kg^{-1} under the starting DIC concentration. Ω_{Ar} increased to ~16.7 after 2 hours, followed by a rapid drop to ~3.2 on day 1 and ~2.0 on day 14, while slightly increasing the following 34 days, varying between 2.0 and 2.1 (Figure 4f).

Concerning ΔTA, ΔDIC and Ω_{Ar}, the 10 minutes and 1 hour dilutions showed similar responses, as did the 1 day and 1 week dilutions. Upon dilution, ΔTA reached values of ~240 µmol kg^{-1} after the 10 minutes and 1 hour dilutions, and about -160 to -190 µmol kg^{-1} for the 1 day and 1 week dilutions. With the exception of one data point in the 1 week dilution data, ΔTA remained relatively constant throughout all dilution experiments (Figure 4d). DIC changes were similar to the TA changes, slowly increasing over time between 0.6 and 2.5 µmol kg^{-1} per day on average, with very similar values reached for the 10 minutes and 1 hour dilutions, as opposed to the 1 day and 1 week ones (Figure 4e). Finally, Ω_{Ar} dropped from ~5.0-5.1 to ~4.0-4.1 over time in the 10 minutes and 1 hour dilutions, while it decreased from ~2.3-2.8 to ~2.1-2.2 until day 21 in the 1 day and 1 week dilution, before increasing to ~2.6-3.4 toward the end of the experiments (Figure 4f).

3.6 Particulate inorganic carbon

With the exception of the ~1050 TA addition by Na$_2$CO$_3$ plus quartz particles, measured PIC in experiments was always higher than estimates from measured ΔTA (Table 2). Furthermore, PIC estimated from the theoretical maximum TA increase upon full mineral dissolution, ΔTA$_{Theo}$, was always higher than estimated PIC from ΔTA, by about 7 to 14% in the ~500 µmol kg^{-1} TA additions with Ca(OH)$_2$ and CaO, respectively, and up to 67% in the experiment with ~2000 µmol kg^{-1} TA additions.

4 Discussion

This study presents the first results on the dissolution of CaO and Ca(OH)$_2$ in natural seawater in the context of ocean alkalinity enhancement. In some of our experiments with at least 500 µmol kg^{-1} TA increase, secondary precipitation was detected via TA and DIC decreases, as well as PIC increases. More specifically, at TA additions leading to an Ω_{Ar} higher than 7 (in the +500 and +1000 µmol kg^{-1} TA treatments), we observed "runaway CaCO$_3$ precipitation", i.e., not only was the added TA completely removed, but significant portions of residual seawater TA as well, until a new steady state was reached. This would vastly reduce the desired CO$_2$ removal potential by OAE and should therefore be avoided. In a subsequent set of experiments, we simulated ocean mixing to test the required timescales to avoid and/or stop secondary CaCO$_3$ precipitation for applications that initially have TA additions above the critical threshold.

4.1 Identifying CaCO$_3$ precipitation, the problem of unmeasured precipitation, and CO$_2$ gas exchange

CaCO$_3$ precipitation can occur via three pathways, i.e., heterogeneous, homogeneous and pseudo-homogeneous nucleation and precipitation (Chen et al., 2005; Marion et al., 2009; Wolf et al., 2008). Heterogeneous precipitation relies on the presence of existing solid mineral phases. This differs from homogeneous precipitation, characterised by the formation of CaCO$_3$ crystals from Ca^{2+} and CO$_3^{2-}$ ions in the absence of any nucleation surfaces (Chen et al., 2005; Wolf et al., 2008). Finally, the last type of precipitation, termed pseudo-homogeneous, is similar to homogeneous nucleation, however it occurs on nuclei other than solid minerals such as colloids, organic particles or glassware in a laboratory setting (Marion et al., 2009).

Concerning the Ω_{CaCO_3} thresholds above which $CaCO_3$ precipitation is expected to occur, the lowest would be for heterogeneous and the highest for homogeneous, with pseudo-homogeneous nucleation in between. This is because nucleation sites effectively lower the activation energy required for $CaCO_3$ precipitation (Morse et al., 2007).

340   When 1 mole of $CaCO_3$ is precipitated, the TA of the solution decreases by 2 moles because of the removal of 1 mole of CO_3^{2-} ions which accounts for 2 moles of TA (Zeebe and Wolf-Gladrow, 2001). Simultaneously, the loss of 1 mole of CO_3^{2-} ions decrease the DIC concentration by 1 mole. Hence, any loss of TA and DIC following a 2:1 ratio can be linked to $CaCO_3$ precipitation (Zeebe and Wolf-Gladrow, 2001). Additionally, when $CaCO_3$ precipitation was suspected in our experiments, SEM and particulate inorganic carbon samples were taken to confirm the presence of $CaCO_3$ and to identify which

345   morphotypes were predominant. In the +250 µmol kg^{-1} TA additions by CaO and $Ca(OH)_2$, both appeared to fully dissolve without inducing $CaCO_3$ precipitation, as TA and Ω_{Ar} quickly increased within minutes, similarly to what has been described in the literature (Chave and Suess, 1970; Rushdi et al., 1992), until reaching their respective maximum after about a day and remaining stable over weeks (Figure 1a and 1c, Figure 2a and 2c). A slight increase in DIC was observed over time, expected when atmospheric CO_2 is ingassing from the bottle headspace, which was created by removing between 150 and 200 mL each

350   sampling point. The measured TA increase was slightly below the theoretically expected increase, which was most likely due to a combination of impurities present (in the case of CaO, a significant fraction could be hydrated), and any loss of the finely ground material during the weighing and sieving process. On average, ~23% of alkalinity added was not detected in the experiments with CaO, and about 14% in the experiments with $Ca(OH)_2$ (Table 1, Figure 1 and Figure 2).

    In contrast, in the +500 µmol kg^{-1} TA additions by CaO and $Ca(OH)_2$, TA started decreasing after about a day, upon the

355   initial increase. If this TA loss was by $CaCO_3$ precipitation, DIC should be reduced by half this amount. And indeed, measured DIC loss was very close to this 2:1 ratio in both the CaO and $Ca(OH)_2$ experiments with a TA addition of 500 µmol kg^{-1} (950:465 and 860:395 for CaO and $Ca(OH)_2$, respectively). This suggests that TA was precipitated in the form of $CaCO_3$. The slight off-set can be explained by ingassing of CO_2 from the head space which would lower the TA:DIC ratio, becoming visible when precipitation ceases towards the end (Figure 1b). Another caveat is the fact that the maximum increase in TA from full

360   dissolution of CaO or $Ca(OH)_2$ cannot be measured in the presence of concurrent $CaCO_3$ precipitation. This is mostly evident in the +2000 µmol kg^{-1} TA addition (Figure 4), where DIC decreases due to $CaCO_3$ precipitation, yet TA increases due to higher $Ca(OH)_2$ dissolution rates. It also explains why estimated PIC calculated from measured TA changes is generally smaller than actually measured PIC concentrations (Table 2). In the experiment with 1M Na_2CO_3 and quartz particles, the measured TA-based PIC estimates however, were larger than the measured PIC. This is difficult to explain, although we

365   observed a white layer on the bottle walls, indicative of $CaCO_3$ precipitation. However, this was also observed during the other experiments with $CaCO_3$ precipitation, yet measured PIC concentrations were larger than when estimated from the TA decrease. In any case, while being a laboratory artefact, this has no practical consequences as in a natural setting the TA would eventually precipitate in the water column. In summary, trying to estimate $CaCO_3$ precipitation from measured changes in TA, without knowing how much TA was actually generated by full mineral dissolution or actual PIC measurements, might

370   underestimate total precipitation.

4.2 The presence of mineral phases triggers "runaway CaCO₃ precipitation"

An important finding in our experiments was that whenever $CaCO_3$ precipitation was observed, it continued even if the solution dropped below an Ω_{Ar} of ~4-5, levels at which no precipitation was observed in the +250 µmol kg⁻¹ TA addition experiments. We termed this phenomenon "runaway precipitation". Furthermore, in all these experiments, precipitation decreased and seemingly ceased at a Ω_{Ar} of ~1.8-2.0. It therefore appears that when $CaCO_3$ is initially precipitated, $CaCO_3$ continues to precipitate in a runaway fashion, even if Ω_{Ar} drops below levels where precipitation would not be initiated in natural seawater. This is to be expected as $CaCO_3$ precipitates onto $CaCO_3$ mineral phases at any saturation state above 1, and the initial precipitation at high saturation states provides new nucleation sites (Morse et al., 2007; Morse et al., 2003; Zhong and Mucci, 1989). The precipitation rate is directly proportional to Ω_{CaCO3}, decreasing exponentially until reaching zero at an Ω_{CaCO3} value of 1 (Figure A 4). However, the question of why precipitation occurred at a much lower Ω_{CaCO3} than anticipated (i.e., Ω_{CaCO3} ~7.5 vs ~12.3) remains (Marion et al., 2009).

It is known that the presence of particles in suspension can initiate and accelerate $CaCO_3$ precipitation (Millero et al., 2001; Morse et al., 2003; Wurgaft et al., 2021). It is unlikely that the presence of $CaCO_3$ impurities in CaO (less than 1% carbon) and $Ca(OH)_2$ (less than 2% carbon) from imperfect calcination would have caused precipitation, as the presence of $CaCO_3$ mineral phases should have caused precipitation at any saturation state above 1, i.e., also in the +250 µmol kg⁻¹ TA addition experiments. Furthermore, modelling precipitation using experimentally determined Ω_{Ar} and surface area dependant aragonite precipitation rates onto $CaCO_3$ mineral phases (Zhong and Mucci, 1989), suggests that once precipitation becomes analytically detectable, it should proceed very rapidly before levelling off (Figure A 5). Furthermore, while we expected $CaCO_3$ precipitation to stop at an Ω_{Ar} ~1, we observed it to stop at Ω_{Ar} of ~2. The presence of dissolved organic carbon could have been slowing down if not stopping $CaCO_3$ precipitation at an Ω_{Ar} higher than 1 (Chave and Suess, 1970; Pan et al., 2021). We also observed that the bulk of precipitation occurred over a period of at least a week, after which an equilibration was reached with apparent differences between the different dissolving minerals (i.e., CaO, $Ca(OH)_2$ and quartz, although it is acknowledged that the experiments were not replicated).

Another explanation for $CaCO_3$ precipitation is heterogeneous precipitation on not yet dissolved CaO and $Ca(OH)_2$ particles (or other impurities), leading to $CaCO_3$ crystal formation and initiating runaway precipitation. The Ω_{Ar} threshold for this process would depend on lattice compatibility of the mineral phases (Tang et al., 2020). For instance, $CaCO_3$ precipitation has been observed at any saturation state above 1 when introducing $CaCO_3$ seed particles. In contrast, Lioliou et al. (2007) did not report $CaCO_3$ precipitation onto quartz particles at an Ω_{Ar} lower than 3.5, and in order to trigger $CaCO_3$ precipitation onto quartz particles, Ω_{Ar} would need to be further increased. Here, we indeed observed $CaCO_3$ precipitation at an Ω_{Ar} of ~9.2 (Figure 3). The reason for an initially slower but then more rapid precipitation could be a combination of exponentially increasing $CaCO_3$ surface area, as well as concomitantly increasing lattice compatibility (Lioliou et al., 2007; Pan et al., 2021). The filtration of TA enriched seawater supports this idea, since not yet dissolved mineral phases that could facilitate early nucleation are removed, preventing runaway $CaCO_3$ precipitation (Figure 3).

Needle-shaped aragonite precipitation onto quartz particles (Figure 5c and 5d) was directly observed by SEM imaging. EDX analyses identified the larger mineral to be rich in silicon, a key characteristic of quartz, and the needle-shaped particles composed of carbon, oxygen and calcium, indicative for $CaCO_3$ (Chang et al., 2017; Ni and Ratner, 2008; Pan et al., 2021). In contrast, direct aragonite precipitation onto not yet dissolved CaO and $Ca(OH)_2$ in the +500 µmol kg^{-1} TA addition is difficult to prove as EDX analyses revealed the presence of Ca and O, both present in the mineral feedstocks and aragonite (Figure 5a and 5b). Finally, in some situations (Figure 5b), round crystals were also observed, suggesting the presence of vaterite (Chang et al., 2017). However, aragonite crystals represented the majority of $CaCO_3$ observed by SEM.

4.3 Impacts of $CaCO_3$ precipitation on OAE potential

From an OAE perspective, $CaCO_3$ precipitation is an important chemical reaction that needs to be avoided. During $CaCO_3$ precipitation, dissolved $[CO_3^{2-}]$ and Ω_{CaCO_3} are decreasing, and $[CO_2]$ is increasing, which reduces the ocean's uptake capacity for atmospheric CO_2, hence impacting OAE potential. Considering typical open ocean TA and DIC concentrations of 2350 and 2100 µmol kg^{-1} respectively, at a salinity of 35 and a temperature of 19 °C, this water mass would have a pCO$_2$ close to atmospheric equilibrium of 416 µatm, a pH$_T$ value (total scale) of 8.04, and an Ω_{Ar} of 2.80. Without $CaCO_3$ precipitation, an addition of 500 µmol kg^{-1} TA would lower pCO$_2$ to ~92 µatm and increase pH$_T$ and Ω_{Ar} to about 8.61 and 8.45 respectively. If fully re-equilibrated with the atmosphere, DIC would increase by about 420 µmol kg^{-1}, leading to a pH$_T$ and Ω_{Ar} 0.07 and 1.10 higher than prior to the addition, respectively (Table 3). The resulting OAE efficiency would be 0.83 mole of atmospheric CO_2 absorbed per mole of TA, very similar to estimates by Köhler et al. (2010). Considering that $CaCO_3$ is the source material for CaO and $Ca(OH)_2$, and the fact that 2 moles of TA are produced per mole of mineral dissolution, ~0.7 tonnes of CO_2 could be captured per tonne of source material, assuming CO_2 capture during the calcination process. At a global-scale, using all available ship capacity and assuming a slow discharge of 1.7 to 4.0 Gt of $Ca(OH)_2$ per year (Caserini et al., 2021), between 1.2 and 2.8 Gt of CO_2 per year could be absorbed by the ocean. Including direct coastal TA discharge at a constant addition of $Ca(OH)_2$ at 10 Gt year^{-1} (Feng et al., 2016), we could expect to absorb an additional 7 Gt of CO_2 per year. To put these model-derived numbers into perspective, the global cement industry currently produces about 4.1 Gt of cement per year (Statista, 2021). Depending on whether hydraulic ($4CaO \cdot Al_2O_3 \cdot Fe_2O_3$) or non-hydraulic ($Ca(OH)_2$) cement is being produced, and assuming a molar Ca^{2+} to CO_2 sequestration potential of 1.6, up to 3.9 Gt of atmospheric CO_2 could be captured per year. This is on the order required to be built-up in the next 30 years, based on the shared socioeconomic pathways RCP2.6 scenario that would keep global warming below the 2 °C target (Huppmann et al., 2018).

However, these numbers can only be obtained when dissolution is complete without $CaCO_3$ precipitation. Hypothetically, if as much $CaCO_3$ precipitates as TA was added, only 1 instead of 1.6 moles of DIC can be absorbed per 2 moles of TA after equilibration with atmospheric pCO$_2$ (Table 3). This represents a decrease by nearly 40% in OAE potential. Similarly, runaway $CaCO_3$ precipitation until an Ω_{Ar} of 2.0, as observed here, decreases the OAE potential further by almost 90%. Then, only ~0.11 mole of DIC would be absorbed per mole of TA added (Table 3). Furthermore, secondary $CaCO_3$ precipitation higher than TA addition will lead to pH$_T$ and Ω_{CaCO_3} levels lower than initial ones. For instance, runaway precipitation for a TA

addition of 500 µmol kg^{-1} will see pH$_T$ drop by about 0.1 from 8.04 to 7.93 and Ω_{Ar} from 2.80 to 1.66, significantly enhancing ongoing ocean acidification (Table 3). Runaway CaCO$_3$ precipitation for a TA addition of 1000 µmol kg^{-1} (assumed to cease at an Ω_{Ar} of 2 as observed here) would even see Ω_{Ar} drop further, i.e., to below 1, upon CO$_2$ re-equilibration with the atmosphere

440   (Table 3). Under such conditions, aragonite would start to dissolve, impacting various living beings, as it is an important biomineral for a variety of marine organisms, e.g., sessile corals, benthic molluscs and planktonic pteropods (Riebesell et al., 2011; Zeebe and Wolf-Gladrow, 2001). In summary, runaway CaCO$_3$ precipitation in OAE has to be avoided as not only reducing CO$_2$ uptake efficiency significantly but also capable of enhancing ocean acidification. Keeping track of OAE efficiency from changes in TA concentrations can be challenging as CaCO$_3$ precipitation can be underestimated as described

445   earlier, requiring new and clever monitoring strategies.

4.4 Avoiding CaCO$_3$ precipitation by dilution and other TA addition strategies

An important aspect when it comes to avoiding CaCO$_3$ precipitation is the dilution that would occur in the wake of ships releasing TA in the ocean, or by natural mixing of TA-enriched water with surrounding seawater (Caserini et al., 2021; Feng et al., 2017; Mongin et al., 2021). In our experiments, a 1:1 dilution could seemingly stop CaCO$_3$ precipitation in seawater, even if performed only after one week for the +500 µmol kg^{-1} TA addition. At a first glance, this comes at a surprise as precipitation nuclei would only be diluted by half, hence reducing surface area and precipitation rates by a factor of 2. However, as Ω_{Ar} is significantly reduced simultaneously, precipitation rates are further reduced by a factor of 10 (see Figure A 4). Hence, overall precipitation would see a reduction by a factor of 20. This should slow down continuing precipitation initially, if on CaCO$_3$ particles, but not completely inhibit it (Zhong and Mucci, 1989). A possible explanation could be that dilution would

455   have lowered Ω_{Ar} below the critical threshold for overcoming lattice mismatch, as most of the aragonite precipitation appears to be on the original seed mineral itself rather than on the newly formed aragonite (compare Figure 5c and 5d).

Overall, CaCO$_3$ precipitation could be avoided if the TA+500 µmol kg^{-1} enriched seawater is diluted 1:1, reaching an Ω_{Ar} of ~5.0. The quicker dilution takes place, the less CaCO$_3$ would precipitate prior. Similar results were found for a TA addition of +2000 µmol kg^{-1}, i.e., the ability to stop precipitation at an Ω_{Ar} of ~5.0, after a 1:7 dilution. However, only the 10 minutes

460   and 1 hour dilutions seem to be suitable in an OAE context, as much more rapidly occurring aragonite precipitation at a higher initial Ω_{Ar} of about 16.7 would significantly reduce the CO$_2$ uptake efficiency. Furthermore, the difficulty to monitor precipitation from simple TA measurements (as described above) would also mean that quantification of CO$_2$ removal is not straight-forward. Hence, in order to assign carbon credits, TA additions have to be done in a way that rule out or at least minimise secondary CaCO$_3$ precipitation. This is true for any type of TA addition, and is not specific to quick and hydrated

465   lime.

Adding TA from land, as modelled by Feng et al. (2017), shows that the more TA is added, the higher coastal Ω_{Ar} would be. By staying clearly below the Ω_{Ar} threshold identified here, i.e., limiting coastal Ω_{Ar} to only 3.2, up to ~550 Gt of carbon in the form of CO$_2$ could be removed from the atmosphere by 2100, corresponding to a reduction by about 260 ppm (Feng et al., 2017). The critical Ω_{Ar} threshold beyond which secondary CaCO$_3$ precipitation would be observed could be higher for other

470 minerals, theoretically allowing for higher TA additions. However, it has to be kept in mind that in waters with high sediment load, often found in coastal settings, $CaCO_3$ could precipitate onto other mineral particles than those added to increase TA. This has been observed in river plumes (Wurgaft et al., 2021), on the Bahama Banks by resuspended sediments (Bustos-Serrano et al., 2009) and in the Red Sea following flash flood deposition of resuspended sediments and particles (Wurgaft et al., 2016). Hence, even with minerals potentially allowing for higher TA additions, an Ω_{Ar} threshold of 5 might be safer to

475 adopt. However, atmospheric CO_2 removal could be increased if TA would also be added to the open ocean, e.g., on ships of opportunity. Here, additions could be much higher as ship movement and rapid mixing within its wake would significantly dilute added TA (Caserini et al., 2021; Köhler et al., 2013) as opposed to coastal point sources.

Finally, another option to increase atmospheric CO_2 uptake would be to not add minerals to seawater directly, but to keep the seawater equilibrated with air or CO_2 enriched flue gases, during mineral dissolution. Firstly, this would allow reaching an

480 Ω_{Ar} of 5 as opposed to 3.3 in the +250 µmol kg^{-1} TA scenario (Table 3), when equilibration occurs after instead of during the dissolution process. And secondly, when reaching an Ω_{Ar} of 5 with CO_2 equilibration, nearly 1000 instead of 250 µmol kg^{-1} of TA could be added, allowing for almost 4 times the amount of atmospheric CO_2 to be removed (this number is highly sensitive to temperature, and ranges between ~3 and ~6 between 30 and 5 °C). However, this represent an extra step, which appears to be far more time and cost consuming than a simple mineral addition. It has also to be kept in mind that for the same Ω_{Ar}

485 threshold, the amount of TA that can be added will increase with lower temperature, as of higher CO_2 solubility and hence naturally lower Ω_{Ar} in colder waters. Based on our Ω_{Ar} threshold of 5, at a salinity of 35 and at 5 °C, about three times as much TA can be dissolved as opposed to a temperature of 30 °C.

5 Conclusions

Ocean alkalinity enhancement is a negative emission technology with relatively large potential for atmospheric CO_2

490 removal (Caserini et al., 2021; Feng et al., 2016; Köhler et al., 2010). In order to maximise carbon dioxide (CO_2) uptake efficiency, secondary calcium carbonate ($CaCO_3$) precipitation has to be avoided. Here, we show that an increase of total alkalinity (TA) by 500 µmol kg^{-1} led to aragonite precipitation, reducing the CO_2 uptake potential from about 0.8 moles per mole of alkalinity added to less than 0.2 moles. Precipitation most likely occurred onto the CaO and Ca(OH)$_2$ mineral phases prior to their full dissolution. In contrast, an addition of 250 µmol kg^{-1} of TA did not result in $CaCO_3$ precipitation, suggesting

495 that an aragonite saturation state (Ω_{Ar}) of about 5 is a safe limit. This is probably also the case for other minerals with even lower lattice compatibility for $CaCO_3$, because in coastal settings, $CaCO_3$ could precipitate onto naturally present mineral phases, such as resuspended sediments. Safely increasing the amount of TA that could be added to the ocean could be achieved by allowing for major mixing and dilution of enriched seawater by coastal tides or in the wake of ships, equilibrating the seawater to atmospheric CO_2 levels prior to the addition during mineral dissolution, and/or targeting low rather than high

500 temperature regions.

Data availability

Data will be made available on a publicly available repository upon final publication.

Author contributions

CAM and KGS designed the initial experiments. All co-authors contributed to the initial data analysis and designing of follow-up experiments. CAM performed most of the sampling, and the data analyses with the help of KGS. CAM wrote the paper with KGS, with inputs from their respective fields of expertise by all co-authors.

Competing interests

The authors declare that they have no conflict of interest.

Acknowledgements

We would like to thank Marian Bailey for her help with ICPMS sample preparation, as well as Dr Nick Ward for his help with preliminary X-ray Diffraction analyses of the calcium powders. We are also thankful to Dr Matheus Carvalho de Carvalho for the particulate carbon analyses and Nadia Toppler for her help arranging the use of the SEM.

Financial support

This research is part of the PhD project of CAM that is funded by a Cat. 5 – SCU Grad School scholarship from the Southern Cross University, Lismore, Australia. The ICPMS analyses were made possible by the Australian Research Council grants number LE200100022 by RJB and KGS, and LE120100201 obtained by RJB.

References

520 Bach, L. T., Gill, S., Rickaby, R., Gore, S., and Renforth, P.: CO2 removal with enhanced weathering and ocean alkalinity enhancement: Potential risks and co-benefits for marine pelagic ecosystems, Frontiers in Climate, 1, 7, 2019.

Bates, N., Best, M., Neely, K., Garley, R., Dickson, A., and Johnson, R.: Detecting anthropogenic carbon dioxide uptake and ocean acidification in the North Atlantic Ocean, Biogeosciences Discussions, 9, 2012.

Berner, R.: The role of magnesium in the crystal growth of calcite and aragonite from sea water, Geochimica et Cosmochimica Acta, 39, 525 489-504, 1975.

Boyd, P., Vivian, C., Boettcher, M., Chai, F., Cullen, J., Goeschl, T., Lampitt, R., Lenton, A., Oschlies, A., and Rau, G.: High level review of a wide range of proposed marine geoengineering techniques, 2019.

Burt, D. J., Fröb, F., and Ilyina, T.: The sensitivity of the marine carbonate system to regional ocean alkalinity enhancement, Frontiers in Climate, 3, 2021.

530 Bustos-Serrano, H., Morse, J. W., and Millero, F. J.: The formation of whitings on the Little Bahama Bank, Marine Chemistry, 113, 1-8, 2009.

Canadell, J. G., Le Quéré, C., Raupach, M. R., Field, C. B., Buitenhuis, E. T., Ciais, P., Conway, T. J., Gillett, N. P., Houghton, R., and Marland, G.: Contributions to accelerating atmospheric CO2 growth from economic activity, carbon intensity, and efficiency of natural sinks, Proceedings of the national academy of sciences, 104, 18866-18870, 2007.

Carter, B. R., Feely, R. A., Wanninkhof, R., Kouketsu, S., Sonnerup, R. E., Pardo, P. C., Sabine, C. L., Johnson, G. C., Sloyan, B. M., and Murata, 535 A.: Pacific anthropogenic carbon between 1991 and 2017, Global Biogeochemical Cycles, 33, 597-617, 2019.

Caserini, S., Pagano, D., Campo, F., Abbà, A., De Marco, S., Righi, D., Renforth, P., and Grosso, M.: Potential of Maritime Transport for Ocean Liming and Atmospheric CO2 Removal, Frontiers in Climate, 3, 22, 2021.

Chang, R., Kim, S., Lee, S., Choi, S., Kim, M., and Park, Y.: Calcium carbonate precipitation for CO2 storage and utilization: a review of the carbonate crystallization and polymorphism, Frontiers in Energy Research, 5, 17, 2017.

540 Chave, K. E. and Suess, E.: Calcium Carbonate Saturation in Seawater: Effects of Dissolved Organic Matter 1, Limnology and Oceanography, 15, 633-637, 1970.

Chen, T., Neville, A., and Yuan, M.: Calcium carbonate scale formation—assessing the initial stages of precipitation and deposition, Journal of Petroleum Science and Engineering, 46, 185-194, 2005.

Cyronak, T., Schulz, K. G., Santos, I. R., and Eyre, B. D.: Enhanced acidification of global coral reefs driven by regional biogeochemical 545 feedbacks, Geophysical Research Letters, 41, 5538-5546, 2014.

De Choudens-Sanchez, V. and Gonzalez, L. A.: Calcite and aragonite precipitation under controlled instantaneous supersaturation: elucidating the role of CaCO3 saturation state and Mg/Ca ratio on calcium carbonate polymorphism, Journal of Sedimentary Research, 79, 363-376, 2009.

Dickson, A. and Millero, F. J.: A comparison of the equilibrium constants for the dissociation of carbonic acid in seawater media, Deep Sea 550 Research Part A. Oceanographic Research Papers, 34, 1733-1743, 1987.

Dickson, A. G.: Standards for ocean measurements, Oceanography, 23, 34-47, 2010.

Dickson, A. G., Sabine, C. L., and Christian, J. R.: Guide to best practices for ocean CO2 measurements, North Pacific Marine Science Organization2007.

Doney, S. C., Fabry, V. J., Feely, R. A., and Kleypas, J. A.: Ocean acidification: the other CO2 problem, Annual review of marine science, 1, 555 169-192, 2009.

Feng, E., Koeve, W., Keller, D. P., and Oschlies, A.: Model-Based Assessment of the CO2 Sequestration Potential of Coastal Ocean Alkalinization, Earth's Future, 5, 1252-1266, 2017.

Feng, E. Y., Keller, D. P., Koeve, W., and Oschlies, A.: Could artificial ocean alkalinization protect tropical coral ecosystems from ocean acidification?, Environmental Research Letters, 11, 074008, 2016.

560 Gafar, N. A. and Schulz, K. G.: A three-dimensional niche comparison of Emiliania huxleyi and Gephyrocapsa oceanica: reconciling observations with projections, Biogeosciences, 15, 3541-3560, 2018.

Gattuso, J.-P., Magnan, A., Billé, R., Cheung, W. W., Howes, E. L., Joos, F., Allemand, D., Bopp, L., Cooley, S. R., and Eakin, C. M.: Contrasting futures for ocean and society from different anthropogenic CO2 emissions scenarios, Science, 349, aac4722, 2015.

González, M. F. and Ilyina, T.: Impacts of artificial ocean alkalinization on the carbon cycle and climate in Earth system simulations, 565 Geophysical Research Letters, 43, 6493-6502, 2016.

Goodwin, P., Brown, S., Haigh, I. D., Nicholls, R. J., and Matter, J. M.: Adjusting mitigation pathways to stabilize climate at 1.5 C and 2.0 C rise in global temperatures to year 2300, Earth's Future, 6, 601-615, 2018.

Harvey, L.: Mitigating the atmospheric CO2 increase and ocean acidification by adding limestone powder to upwelling regions, Journal of Geophysical Research: Oceans, 113, 2008.

570   Hoegh-Guldberg, O., Jacob, D., Taylor, M., Bolaños, T. G., Bindi, M., Brown, S., Camilloni, I., Diedhiou, A., Djalante, R., and Ebi, K.: The human imperative of stabilizing global climate change at 1.5° C, Science, 365, eaaw6974, 2019.

Hoegh-Guldberg, O., Mumby, P. J., Hooten, A. J., Steneck, R. S., Greenfield, P., Gomez, E., Harvell, C. D., Sale, P. F., Edwards, A. J., and Caldeira, K.: Coral reefs under rapid climate change and ocean acidification, science, 318, 1737-1742, 2007.

Huppmann, D., Kriegler, E., Krey, V., Riahi, K., Rogelj, J., Rose, S. K., Weyant, J., Bauer, N., Bertram, C., and Bosetti, V.: IAMC 1.5 C Scenario
575   Explorer and Data hosted by IIASA, Integrated Assessment Modeling Consortium & International Institute for Applied Systems Analysis, 10, 2018.

Ilyina, T., Wolf-Gladrow, D., Munhoven, G., and Heinze, C.: Assessing the potential of calcium-based artificial ocean alkalinization to mitigate rising atmospheric CO2 and ocean acidification, Geophysical Research Letters, 40, 5909-5914, 2013.

IPCC: Climate Change 2021: The Physical Science Basis. Contribution of Working Group I to the Sixth Assessment Report of the
580   Intergovernmental Panel on Climate Change [Masson-Delmotte, V., P. Zhai, A. Pirani, S. L. Connors, C. Péan, S. Berger, N. Caud, Y. Chen, L. Goldfarb, M. I. Gomis, M. Huang, K. Leitzell, E. Lonnoy, J. B. R. Matthews, T. K. Maycock, T. Waterfield, O. Yelekçi, R. Yu and B. Zhou (eds.)]. Cambridge University Press. In Press., 2021.

Keller, D. P., Feng, E. Y., and Oschlies, A.: Potential climate engineering effectiveness and side effects during a high carbon dioxide-emission scenario, Nature communications, 5, 1-11, 2014.

585   Kheshgi, H. S.: Sequestering atmospheric carbon dioxide by increasing ocean alkalinity, Energy, 20, 915-922, 1995.

Köhler, P., Hartmann, J., and Wolf-Gladrow, D. A.: Geoengineering potential of artificially enhanced silicate weathering of olivine, Proceedings of the National Academy of Sciences, 107, 20228-20233, 2010.

Köhler, P., Abrams, J. F., Völker, C., Hauck, J., and Wolf-Gladrow, D. A.: Geoengineering impact of open ocean dissolution of olivine on atmospheric CO2, surface ocean pH and marine biology, Environmental Research Letters, 8, 014009, 2013.

590   Lenton, A., Matear, R. J., Keller, D. P., Scott, V., and Vaughan, N. E.: Assessing carbon dioxide removal through global and regional ocean alkalinization under high and low emission pathways, Earth System Dynamics, 9, 339-357, 2018.

Lenton, T. and Vaughan, N.: The radiative forcing potential of different climate geoengineering options. Atmos. Chem. Phys. Discuss., V, 2009.

Lewis, E. and Perkin, R.: The practical salinity scale 1978: conversion of existing data, Deep Sea Research Part A. Oceanographic Research
595   Papers, 28, 307-328, 1981.

Lioliou, M. G., Paraskeva, C. A., Koutsoukos, P. G., and Payatakes, A. C.: Heterogeneous nucleation and growth of calcium carbonate on calcite and quartz, Journal of colloid and interface science, 308, 421-428, 2007.

Lueker, T. J., Dickson, A. G., and Keeling, C. D.: Ocean pCO2 calculated from dissolved inorganic carbon, alkalinity, and equations for K1 and K2: validation based on laboratory measurements of CO2 in gas and seawater at equilibrium, Marine chemistry, 70, 105-119, 2000.

600   Marion, G., Millero, F. J., and Feistel, R.: Precipitation of solid phase calcium carbonates and their effect on application of seawater SA–T–P models, Ocean Science, 5, 285, 2009.

Mehrbach, C., Culberson, C., Hawley, J., and Pytkowicx, R.: Measurement of the apparent dissociation constants of carbonic acid in seawater at atmospheric pressure 1, Limnology and oceanography, 18, 897-907, 1973.

Millero, F., Huang, F., Zhu, X., Liu, X., and Zhang, J.-Z.: Adsorption and desorption of phosphate on calcite and aragonite in seawater, Aquatic
605   Geochemistry, 7, 33-56, 2001.

Mongin, M., Baird, M. E., Lenton, A., Neill, C., and Akl, J.: Reversing ocean acidification along the Great Barrier Reef using alkalinity injection, Environmental Research Letters, 16, 064068, 2021.

Montserrat, F., Renforth, P., Hartmann, J., Leermakers, M., Knops, P., and Meysman, F. J.: Olivine dissolution in seawater: implications for CO2 sequestration through enhanced weathering in coastal environments, Environmental science & technology, 51, 3960-3972, 2017.

610   Morse, J. W. and He, S.: Influences of T, S and PCO2 on the pseudo-homogeneous precipitation of CaCO3 from seawater: implications for whiting formation, Marine Chemistry, 41, 291-297, 1993.

Morse, J. W., Arvidson, R. S., and Lüttge, A.: Calcium carbonate formation and dissolution, Chemical reviews, 107, 342-381, 2007.

Morse, J. W., Gledhill, D. K., and Millero, F. J.: Caco3 precipitation kinetics in waters from the great Bahama bank:: Implications for the relationship between bank hydrochemistry and whitings, Geochimica et Cosmochimica Acta, 67, 2819-2826, 2003.

615   Morse, J. W., Wang, Q., and Tsio, M. Y.: Influences of temperature and Mg: Ca ratio on CaCO3 precipitates from seawater, Geology, 25, 85-87, 1997.

Mucci, A.: The solubility of calcite and aragonite in seawater at various salinities, temperatures, and one atmosphere total pressure, Am. J. Sci, 283, 780-799, 1983.

National Academies of Sciences, E. and Medicine: A Research Strategy for Ocean-based Carbon Dioxide Removal and Sequestration, The
620   National Academies Press, Washington, DC, 360 pp., doi:10.17226/26278, 2021.

Ni, M. and Ratner, B. D.: Differentiating calcium carbonate polymorphs by surface analysis techniques—an XPS and TOF-SIMS study, Surface and Interface Analysis: An International Journal devoted to the development and application of techniques for the analysis of surfaces, interfaces and thin films, 40, 1356-1361, 2008.

Pan, Y., Li, Y., Ma, Q., He, H., Wang, S., Sun, Z., Cai, W.-J., Dong, B., Di, Y., and Fu, W.: The role of Mg2+ in inhibiting CaCO3 precipitation from seawater, Marine Chemistry, 104036, 2021.

Pytkowicz, R. M.: Rates of inorganic calcium carbonate nucleation, The Journal of Geology, 73, 196-199, 1965.

Renforth, P. and Henderson, G.: Assessing ocean alkalinity for carbon sequestration, Reviews of Geophysics, 55, 636-674, 2017.

Renforth, P. and Kruger, T.: Coupling mineral carbonation and ocean liming, Energy & fuels, 27, 4199-4207, 2013.

Renforth, P., Jenkins, B., and Kruger, T.: Engineering challenges of ocean liming, Energy, 60, 442-452, 2013.

Riebesell, U., Fabry, V. J., Hansson, L., and Gattuso, J.-P.: Guide to best practices for ocean acidification research and data reporting, Office for Official Publications of the European Communities2011.

Riley, J. and Tongudai, M.: The major cation/chlorinity ratios in sea water, Chemical Geology, 2, 263-269, 1967.

Rushdi, A., Pytkowicz, R., Suess, E., and Chen, C.: The effects of magnesium-to-calcium ratios in artificial seawater, at different ionic products, upon the induction time, and the mineralogy of calcium carbonate: a laboratory study, Geologische Rundschau, 81, 571-578, 1992.

Schulz, K. G., Bach, L. T., Bellerby, R. G., Bermúdez, R., Büdenbender, J., Boxhammer, T., Czerny, J., Engel, A., Ludwig, A., and Meyerhöfer, M.: Phytoplankton blooms at increasing levels of atmospheric carbon dioxide: experimental evidence for negative effects on prymnesiophytes and positive on small picoeukaryotes, Frontiers in Marine Science, 4, 64, 2017.

Simkiss, K.: The inhibitory effects of some metabolites on the precipitation of calcium carbonate from artificial and natural sea water, ICES Journal of Marine Science, 29, 6-18, 1964.

Statista: Global cement industry - Statistics & Facts. See: https://www.statista.com/topics/8700/cement-industry-worldwide/, 2021.

Tang, H., Wu, X., Xian, H., Zhu, J., Wei, J., Liu, H., and He, H.: Heterogeneous Nucleation and Growth of CaCO3 on Calcite (104) and Aragonite (110) Surfaces: Implications for the Formation of Abiogenic Carbonate Cements in the Ocean, Minerals, 10, 294, 2020.

The Royal Society and Royal Academy of Engineering.: Greenhouse Gas Removal. See: https://royalsociety.org/-/media/policy/projects/greenhouse-gas-removal/royal-society-greenhouse-gas-removal-report-2018.pdf, 2018.

Uppstrom, L.: The boron/chlorinity ratio of deep-sea water from the Pacific Ocean, Deep Sea Res., 21, 161-162, 1974.

Wolf-Gladrow, D. A., Zeebe, R. E., Klaas, C., Körtzinger, A., and Dickson, A. G.: Total alkalinity: The explicit conservative expression and its application to biogeochemical processes, Marine Chemistry, 106, 287-300, 2007.

Wolf, S. E., Leiterer, J., Kappl, M., Emmerling, F., and Tremel, W.: Early homogenous amorphous precursor stages of calcium carbonate and subsequent crystal growth in levitated droplets, Journal of the American Chemical Society, 130, 12342-12347, 2008.

Wurgaft, E., Steiner, Z., Luz, B., and Lazar, B.: Evidence for inorganic precipitation of CaCO3 on suspended solids in the open water of the Red Sea, Marine Chemistry, 186, 145-155, 2016.

Wurgaft, E., Wang, Z., Churchill, J., Dellapenna, T., Song, S., Du, J., Ringham, M., Rivlin, T., and Lazar, B.: Particle triggered reactions as an important mechanism of alkalinity and inorganic carbon removal in river plumes, Geophysical Research Letters, e2021GL093178, 2021.

Zeebe, R. E. and Wolf-Gladrow, D.: CO2 in seawater: equilibrium, kinetics, isotopes, 65, Gulf Professional Publishing2001.

Zhong, S. and Mucci, A.: Calcite and aragonite precipitation from seawater solutions of various salinities: Precipitation rates and overgrowth compositions, Chemical geology, 78, 283-299, 1989.

Table 1: Summary of experimental conditions. Please note that for comparability, more TA was added in the liquid than the sieved approaches to match the theoretical increases in calcium carbonate saturation state (see Methods section for details).

TA Agent	TA target (μmol kg^{-1})	Comments	Amount added in mg (or mL*)	Amount of natural seawater in kg	mg kg^{-1} (or mL kg^{-1}*)	Theoretical TA addition (μmol kg^{-1})	Recorded TA addition (μmol kg^{-1})	Experiment duration	Additional samples apart from TA and DIC
					Sieved calcium minerals experiments				
CaO	250	Sieved in	15.50	2015.90	7.69	274.21	216.49	47 days	N/A
CaO	500	Sieved in	30.60	2004.50	15.27	544.42	410.70	47 days	TPC, POC and SEM samples
Ca(OH)$_2$	250	Sieved in	19.90	2001.90	9.94	268.34	221.96	28 days	N/A
Ca(OH)$_2$	500	Sieved in	37.40	2004.20	18.66	503.73	440.19	42 days	TPC, POC and SEM samples
					Na$_2$CO$_3$, particles and filtration experiments				
Na$_2$CO$_3$	1050	1M Na$_2$CO$_3$ solution	1.05*	2000.60	0.52	1050.32	1057.41	42 days	N/A
Na$_2$CO$_3$	1050	1M Na$_2$CO$_3$ solution, plus quartz powder after 2 days Sieved in,	1.05*	2000.30	0.5	1050.16	1073.92	48 days	TPC, POC and SEM samples
Ca(OH)$_2$	500	filtered after 4 hours	39.30	2004.30	19.61	529.30	470.79	48 days	N/A
					Dilution experiments				
Ca(OH)$_2$	500	1:1 dilution after 10min, 1 hour, 1 day and 1 week	101.60	5132.50	19.80	534.36	452.65	14 days	TPC, POC and SEM samples
Ca(OH)$_2$	2000	1:7 dilution after 10min, 1 hour, 1 day and 1 week	155.90	2003.80	77.80	2100.21	724.04	48 days	TPC, POC and SEM samples

660

Table 2: Comparison between the estimated PIC based on half the TA change between the theoretical maximum TA increase upon full dissolution of the alkaline material added and the measured TA at the end of the experiment (Table 1), the estimated PIC based on half the TA changes between the measured maximum TA increase and the measured TA at the end of the experiment, and the measured PIC from the particulate carbon analysis.

Experiment	PIC ΔTA_{Theo} ($\mu mol\ kg^{-1}$)	PIC ΔTA ($\mu mol\ kg^{-1}$)	Measured PIC ($\mu mol\ kg^{-1}$)
500 TA – CaO	543.24	476.38	491.82 ±39.18
500 TA – Ca(OH)$_2$	462.28	430.51	550.87 ±71.32
1050 TA – 1M Na$_2$CO$_3$+ Quartz Particles	627.20	639.07	397.37 ±24.03
500 TA – Ca(OH)$_2$ Dilution	107.05	66.20	89.51 ±4.27
2000 TA – Ca(OH)$_2$ Dilution	1718.83	1030.74	1331.48 ±50.73

665

Table 3: Simulations of the changes in TA, DIC, Ω_{Ar}, pCO_2 and pH_T (total scale) after TA increases of 250, 500 and 1000 μmol kg⁻¹, assuming complete mineral dissolution without precipitation, a complete dissolution followed by as much CaCO₃ precipitated as the amount of TA added, and a complete dissolution followed by CaCO₃ precipitation until reaching an Ω_{Ar} of 2.0, before CO₂ re-equilibration to initial pCO₂. For each scenario, the amount of moles of CO₂ absorbed per moles of TA added has been calculated for comparison. The 500 μmol kg⁻¹ TA addition simulation is shown in Figure A 3, Appendix. *Note: the value for Ω_{Ar} is rounded to 1.00 but calculated at 0.997.

	Starting Conditions (salinity = 35 19 °C)	TA +250 μmol kg⁻¹ No CaCO₃ precipitation	TA +500 μmol kg⁻¹ No CaCO₃ Prec.	CaCO₃ Prec. = TA added	CaCO₃ Prec. until Ω_{Ar} of 2	TA +1000 μmol kg⁻¹ No CaCO₃ Prec.	CaCO₃ Prec. = TA added	CaCO₃ Prec. until Ω_{Ar} of 2
TA (μmol kg⁻¹)	2350	2600	2850	2350	1748	3350	2350	1320
DIC (μmol kg⁻¹)	2100	2100	2100	1850	1549	2100	1600	1085
Ω_{Ar}	2.80	5.53	8.45	5.34	2.00	14.57	7.89	2.00
pCO_2 (μatm)	416.2	175.1	91.5	135.6	319.2	29.6	48.2	144.81
pH_T	8.04	8.38	8.61	8.42	8.02	8.97	8.73	8.20
After re-equilibration, i.e., pCO_2 ~416 μatm								
Final TA (μmol kg⁻¹)	2350	2600	2850	2350	1748	3350	2350	1320
Final DIC (μmol kg⁻¹)	2100	2309	2517	2100	1588	2926.5	2100	1216
Final Ω_{Ar}	2.80	3.34	3.90	2.80	1.66	5.14	2.80	1.00*
Final pH_T	8.04	8.08	8.11	8.04	7.93	8.17	8.04	7.82
CO₂ uptake (mole/mole TA)	NA	0.84	0.83	0.50	0.08	0.83	0.50	0.13

670
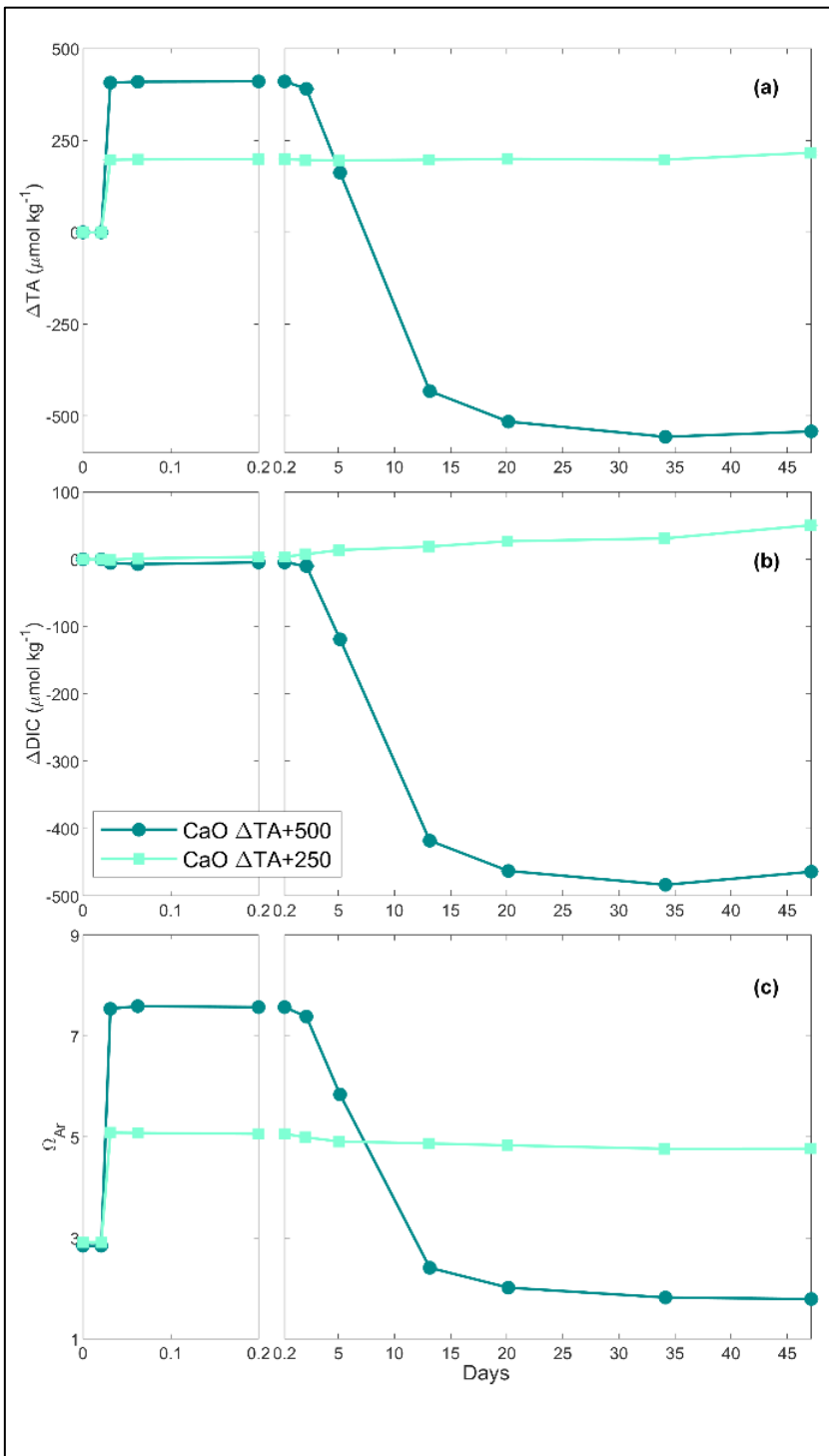
Figure 1: Changes in TA (a), DIC (b) and Ω_{Ar} (c) over time following two CaO additions.
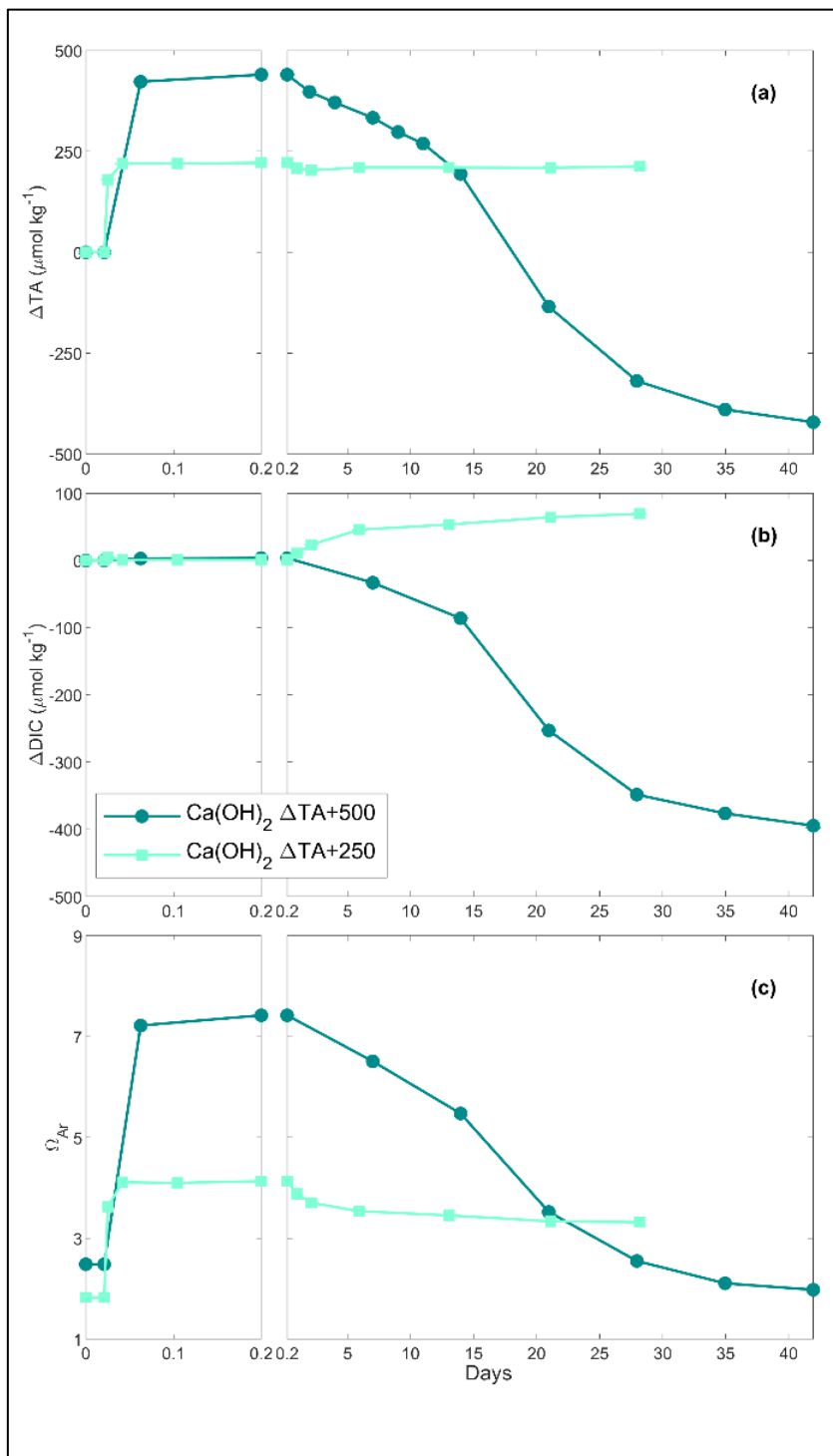
Figure 2: Changes in TA (a), DIC (b) and Ω_{Ar} (c) of the samples over time following two Ca(OH)₂ additions.
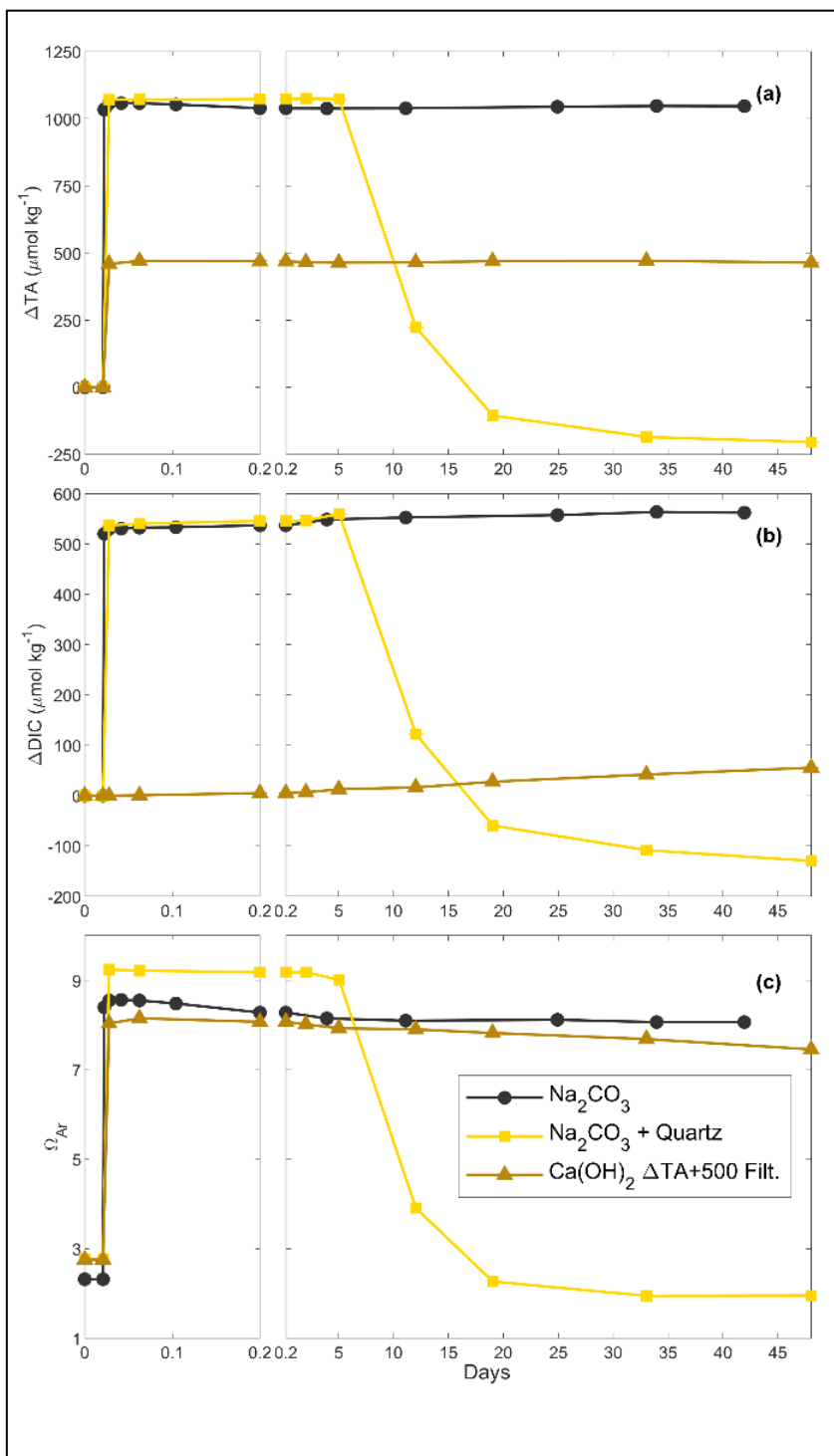
675

Figure 3: Changes in TA (a), DIC (b) and Ω_{Ar} (c) over time following additions of Na_2CO_3, Na_2CO_3 plus quartz particles and $Ca(OH)_2$ followed by a filtration step (see Methods for details).
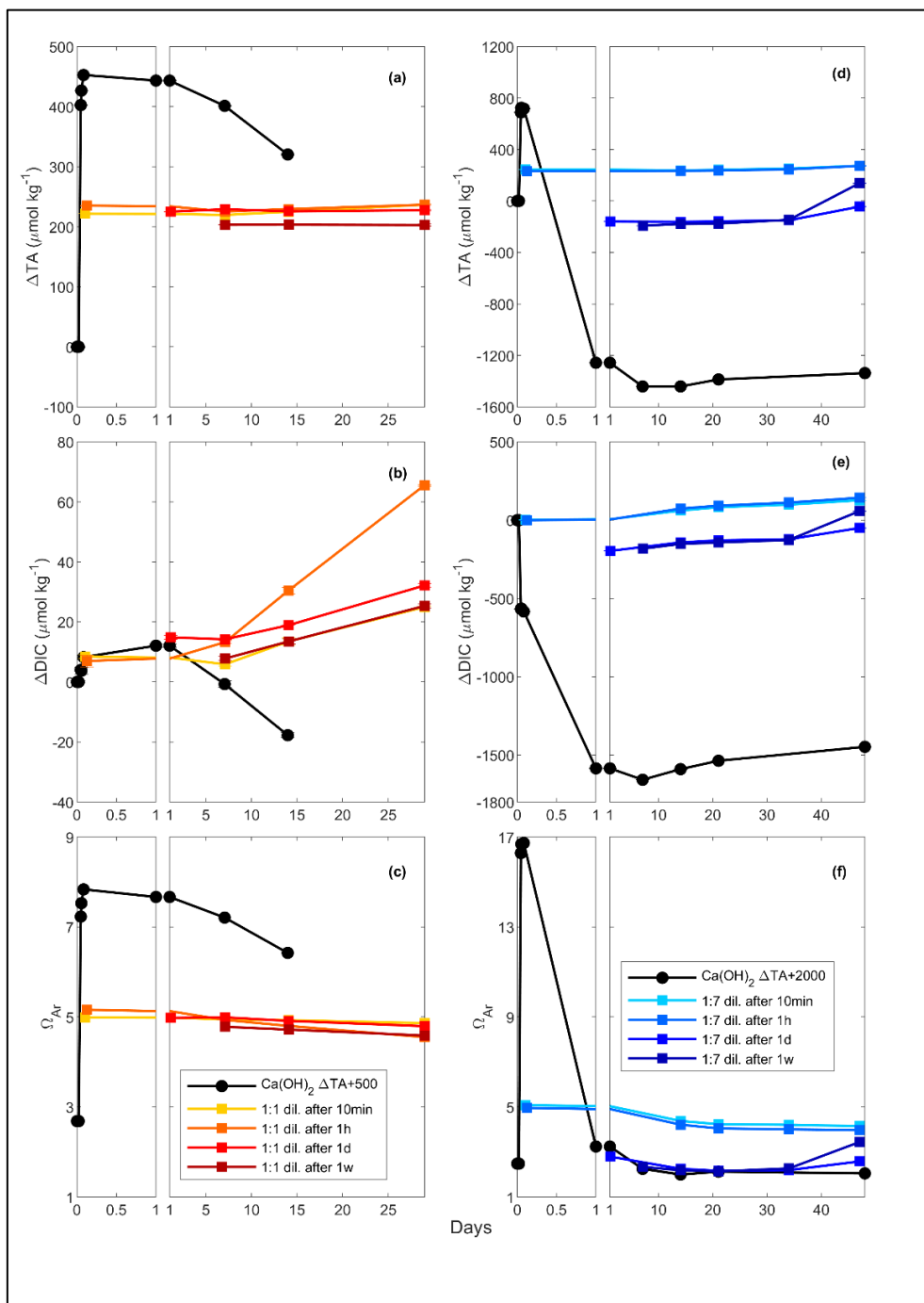
Figure 4: Changes in TA (a and d), DIC (b and e) and Ω_{Ar} (c and f) following a TA addition of 500 and 2000 µmol kg^{-1} respectively, by Ca(OH)$_2$ (black line), as well as following a 1:1 dilution or the 500 µmol kg^{-1} TA addition (red and yellow lines) and a 1:7 dilution for the 2000 µmol kg^{-1} TA addition (blue lines). The dilutions were performed after 10 minutes, 1 hour, 1 day and 1 week and earlier dilutions are represented by lighter colours.
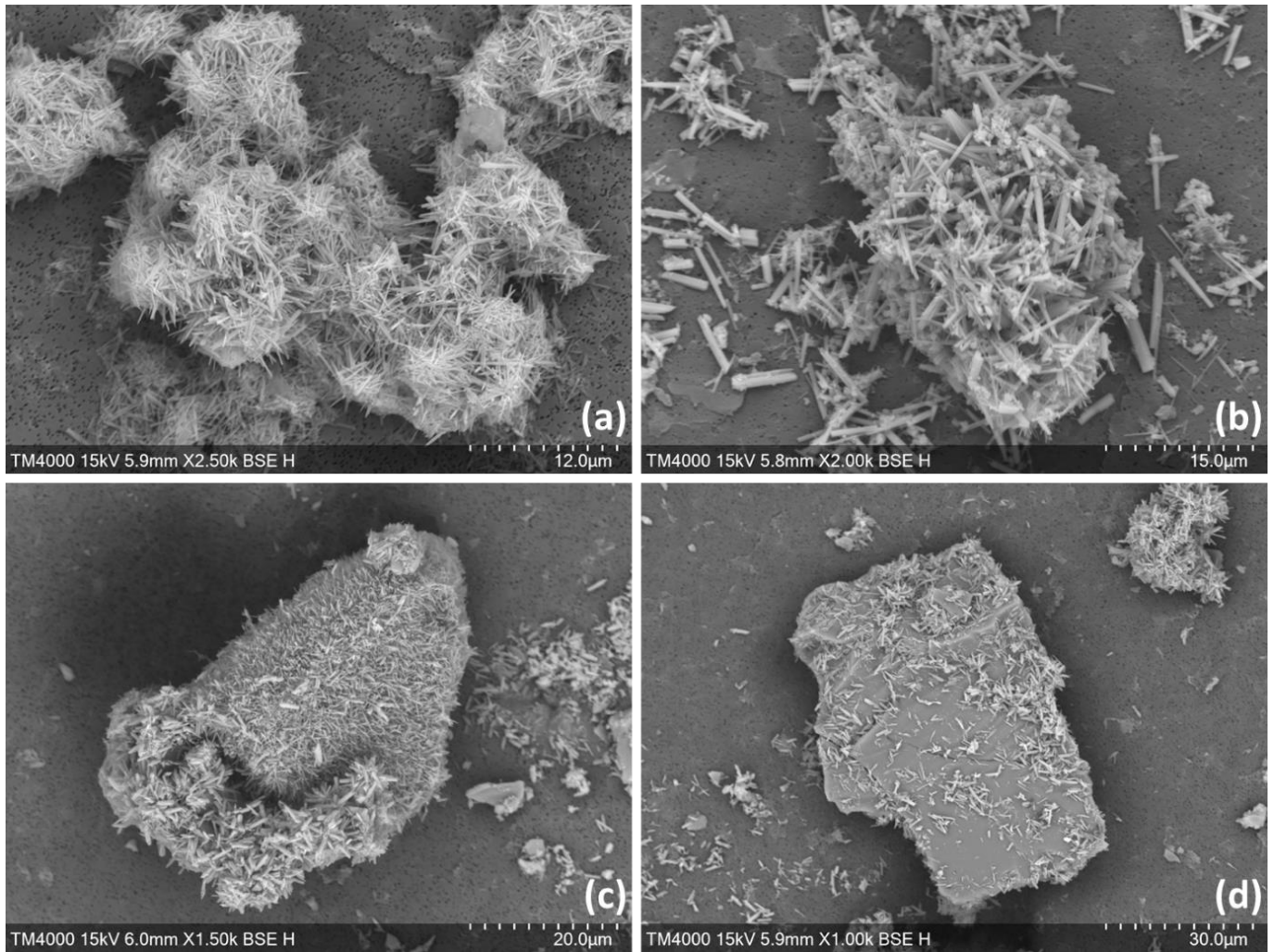
685

Figure 5: SEM images from experiments with an increase in TA of ~500 µmol kg^{-1} by CaO (a), Ca(OH)$_2$ (b) and with a TA increase of ~1050 µmol kg^{-1} by 1M Na$_2$CO$_3$, followed by quartz particles addition ((c) and (d)).

 Appendix

Table A 1: Seawater salinity in each experiment, and phosphate concentrations in one of the batches (*).

Alkaline mineral	TA increase (in μmol kg^{-1})	Experiment details	Seawater salinity	Phosphate (in μmol kg^{-1})*
CaO	250	N/A	36.52	Not measured
	500	N/A	36.52	Not measured
Ca(OH)$_2$	250	N/A	36.91	Not measured
	500	N/A	36.91	Not measured
	500	For dilutions	35.46	Not measured
	500	For filtration	36.52	Not measured
	2000	For dilution	36.74	0.32 ±0.03
Na$_2$CO$_3$	1050	N/A	36.91	Not measured
	1050	With quartz particles	36.52	Not measured

 Table A 2: Main chemical composition of the CaO and Ca(OH)$_2$ feedstocks used for the TA increase experiments determined by ICPMS analysis.

CaO Powder			Ca(OH)$_2$ Powder		
Element	mg g^{-1}	St. Dev.	Element	mg g^{-1}	St. Dev.
Calcium	545.15	70.92	Calcium	529.79	117.30
Magnesium	2.10	0.23	Magnesium	6.87	1.98
Silicon	2.02	1.79	Silicon	2.70	1.12
Aluminium	0.50	0.19	Aluminium	1.98	0.77
Iron	0.32	0.10	Iron	0.91	0.34
Manganese	0.11	0.01	Potassium	0.43	0.23
Potassium	0.03	0.00	Titanium	0.07	0.03
Phosphorus	0.02	0.02	Manganese	0.05	0.01
Titanium	0.02	0.01	Phosphorus	0.04	0.01
Chromium	0.01	0.01	Bromine	0.03	0.01
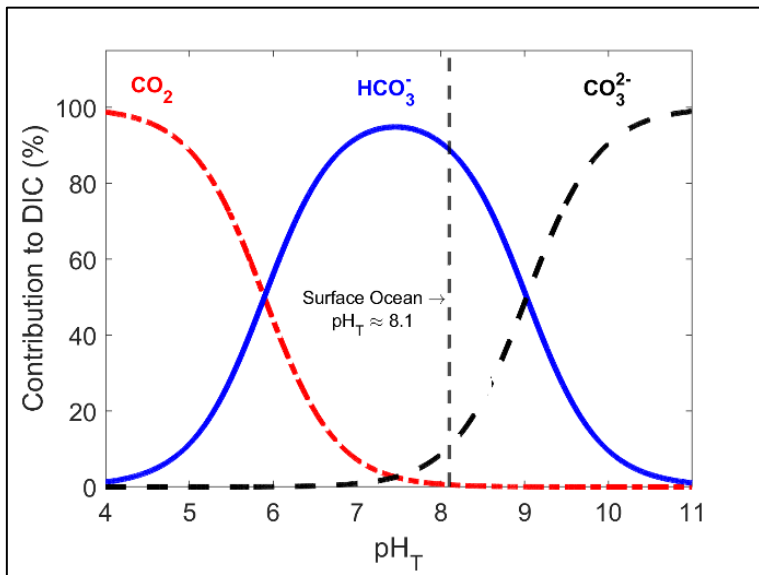
Figure A 1: Relative contribution of dissolved CO_2, HCO_3^- and CO_3^{2-} to total dissolved inorganic carbon in seawater as a function of pH_T (total scale), also known as Bjerrum plot (based on the carbonic acid equilibrium constant from Mehrbach et al. (1973) and refitted by Dickson and Millero (1987)), at 25 °C and salinity of 35, with the current surface ocean pH average represented by the dashed line (pH_T ~8.1).

700
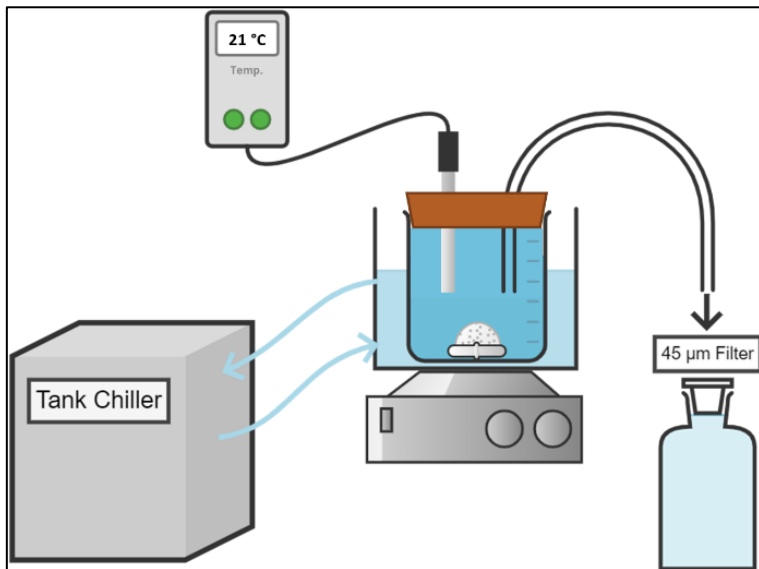
705 **Figure A 2: Conceptual diagram of the experimental setup used for the dissolution of alkaline minerals**
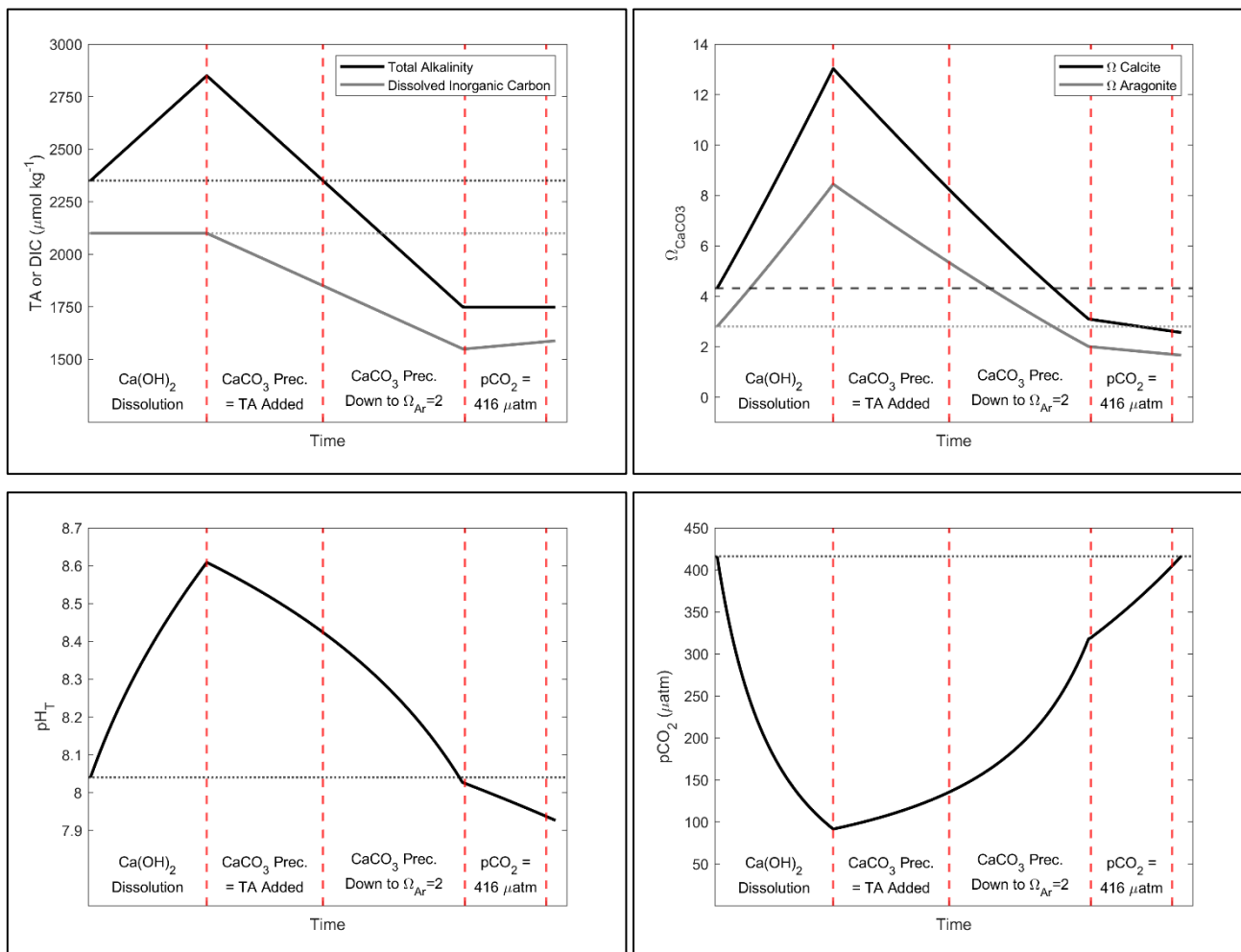
710

Figure A 3: Simulation of the changes in TA, DIC, Ω_{Ca}, Ω_{Ar}, pCO$_2$ and pH$_T$ after addition of 500 µmol kg^{-1} of alkalinity. Four important steps are presented. First, assuming the complete Ca(OH)$_2$ dissolution without CaCO$_3$ precipitation, second, assuming as much CaCO$_3$ precipitation as the amount of TA added, third, assuming CaCO$_3$ precipitation happening until reaching an Ω_{Ar} of 2, and fourth, CO$_2$ uptake until equilibrium is reached between atmosphere and seawater at a pCO$_2$ of ~416 µatm.
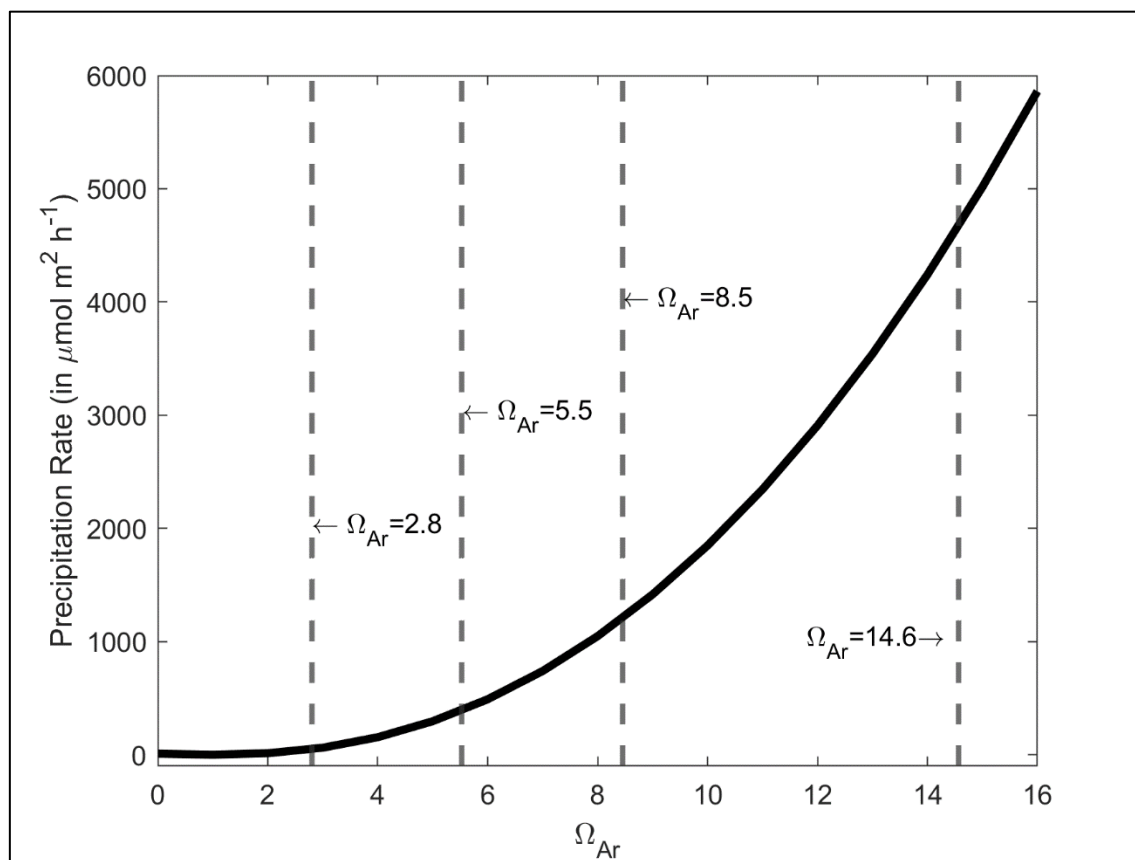
Figure A 4: CaCO₃ precipitation rate onto aragonite seed crystals in μmol m⁻² h⁻¹ as a function of Ω_{Ar}, based on the measurements of Zhong and Mucci (1989) at 25 °C and for a salinity of 35. The Ω_{Ar} values for the starting conditions, and following a +250, +500 and +1000 μmol kg-1 TA increase are presented by the grey dashed lines, i.e., 2.8, 5.5, 8.5 and 14.6 respectively.

720
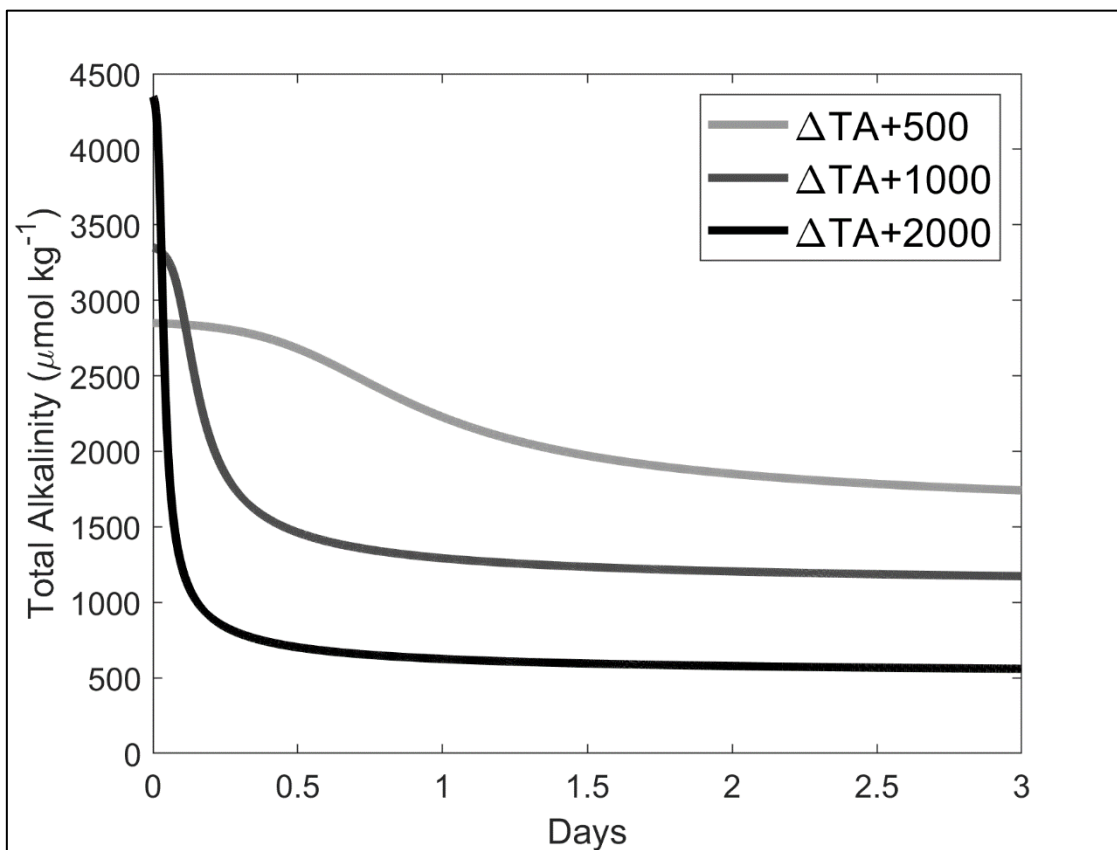
Figure A 5: Simulations of TA loss due to aragonite precipitation after a TA addition of 500, 1000 and 2000 μmol kg⁻¹, based on Ω_{Ar} and surface area dependant precipitation rates shown in Figure A 4, assuming the initial presence of 2% of CaCO₃ in our samples, i.e., ~0.37, ~0.74 and ~1.48 mg kg⁻¹ for a ΔTA+500, ΔTA+1000 and ΔTA+2000 μmol kg⁻¹, respectively. CaCO₃ mass was converted to a surface area as described in Zhong and Mucci (1989). The starting conditioned were TA = 2300 μmol kg⁻¹, DIC = 2100 μmol kg⁻¹, salinity = 35 and temperature = 21 °C.